Pion femtoscopy in p + p collisions at √s=200 GeV

(STAR Collaboration) Aggarwal, M. M.; ...; Planinić, Mirko; ...; Poljak, Nikola; ...; Zoulkarneeva, Y.

Pion femtoscopy in $p + p$ collisions at $\sqrt{s} = 200$ GeV

M. M. Aggarwal,[31] Z. Ahammed,[22] A. V. Alakhverdyants,[18] I. Alekseev,[16] J. Alford,[19] B. D. Anderson,[19] D. Arkhipkin,[3] G. S. Averichev,[18] J. Balewski,[23] L. S. Barnby,[2] S. Baumgart,[53] D. R. Beavis,[3] R. Bellwied,[51] M. J. Betancourt,[23] R. R. Betts,[8] A. Bhasin,[17] A. K. Bhati,[31] H. Bichsel,[50] J. Bielcik,[10] J. Bielcikova,[11] B. Biritz,[6] L. C. Bland,[3] B. E. Bonner,[37] J. Bouchet,[19] E. Braidot,[28] A. V. Brandin,[26] A. Bridgeman,[1] E. Bruna,[53] S. Bueltmann,[30] I. Bunzarov,[18] T. P. Burton,[3] X. Z. Cai,[41] H. Caines,[53] M. Calderón de la Barca Sánchez,[5] O. Catu,[53] D. Cebra,[5] R. Cendejas,[6] M. C. Cervantes,[43] Z. Chajecki,[29] P. Chaloupka,[11] S. Chattopadhyay,[48] H. F. Chen,[39] J. H. Chen,[41] J. Y. Chen,[52] J. Cheng,[45] M. Cherney,[9] A. Chikanian,[53] K. E. Choi,[35] W. Christie,[3] P. Chung,[11] R. F. Clarke,[43] M. J. M. Codrington,[43] R. Corliss,[23] J. G. Cramer,[50] H. J. Crawford,[4] D. Das,[5] S. Dash,[13] A. Davila Leyva,[44] L. C. De Silva,[51] R. R. Debbe,[3] T. G. Dedovich,[18] A. A. Derevschikov,[33] R. Derradi de Souza,[7] L. Didenko,[3] P. Djawotho,[43] S. M. Dogra,[17] X. Dong,[22] J. L. Drachenberg,[43] J. E. Draper,[5] J. C. Dunlop,[3] M. R. Dutta Mazumdar,[48] L. G. Efimov,[18] E. Elhalhuli,[2] M. Elnimr,[51] J. Engelage,[4] G. Eppley,[37] B. Erazmus,[42] M. Estienne,[42] L. Eun,[32] O. Evdokimov,[8] P. Fachini,[3] R. Fatemi,[20] J. Fedorisin,[18] R. G. Fersch,[20] P. Filip,[18] E. Finch,[53] V. Fine,[3] Y. Fisyak,[3] C. A. Gagliardi,[43] D. R. Gangadharan,[6] M. S. Ganti,[48] E. J. Garcia-Solis,[8] A. Geromitsos,[42] F. Geurts,[37] V. Ghazikhanian,[6] P. Ghosh,[48] Y. N. Gorbunov,[9] A. Gordon,[3] O. Grebenyuk,[22] D. Grosnick,[47] S. M. Guertin,[6] A. Gupta,[17] N. Gupta,[17] W. Guryn,[3] B. Haag,[5] A. Hamed,[43] L-X. Han,[41] J. W. Harris,[53] J. P. Hays-Wehle,[23] M. Heinz,[53] S. Heppelmann,[32] A. Hirsch,[34] E. Hjort,[22] A. M. Hoffman,[23] G. W. Hoffmann,[44] D. J. Hofman,[8] B. Huang,[39] H. Z. Huang,[6] T. J. Humanic,[29] L. Huo,[43] G. Igo,[6] P. Jacobs,[22] W. W. Jacobs,[15] C. Jena,[13] F. Jin,[41] C. L. Jones,[23] P. G. Jones,[2] J. Joseph,[19] E. G. Judd,[4] S. Kabana,[42] K. Kajimoto,[44] K. Kang,[45] J. Kapitan,[11] K. Kauder,[8] D. Keane,[19] A. Kechechyan,[18] D. Kettler,[50] D. P. Kikola,[22] J. Kiryluk,[22] A. Kisiel,[49] S. R. Klein,[22] A. G. Knospe,[53] A. Kocoloski,[23] D. D. Koetke,[47] T. Kollegger,[12] J. Konzer,[34] I. Koralt,[30] L. Koroleva,[16] W. Korsch,[20] L. Kotchenda,[26] V. Kouchpil,[11] P. Kravtsov,[26] K. Krueger,[1] M. Krus,[10] L. Kumar,[19] P. Kurnadi,[6] M. A. C. Lamont,[3] J. M. Landgraf,[3] S. LaPointe,[51] J. Lauret,[3] A. Lebedev,[3] R. Lednicky,[18] C-H. Lee,[35] J. H. Lee,[3] W. Leight,[23] M. J. LeVine,[3] C. Li,[39] L. Li,[44] N. Li,[52] W. Li,[41] X. Li,[40] X. Li,[34] Y. Li,[45] Z. M. Li,[52] G. Lin,[53] S. J. Lindenbaum,[27] M. A. Lisa,[29] F. Liu,[52] H. Liu,[5] J. Liu,[37] T. Ljubicic,[3] W. J. Llope,[37] R. S. Longacre,[3] W. A. Love,[3] Y. Lu,[39] E. V. Lukashov,[26] X. Luo,[39] G. L. Ma,[41] Y. G. Ma,[41] D. P. Mahapatra,[13] R. Majka,[53] O. I. Mall,[5] L. K. Mangotra,[17] R. Manweiler,[47] S. Margetis,[19] C. Markert,[44] H. Masui,[22] H. S. Matis,[22] Yu. A. Matulenko,[33] D. McDonald,[37] T. S. McShane,[9] A. Meschanin,[33] R. Milner,[23] N. G. Minaev,[33] S. Mioduszewski,[43] A. Mischke,[28] M. K. Mitrovski,[12] B. Mohanty,[48] M. M. Mondal,[48] B. Morozov,[16] D. A. Morozov,[33] M. G. Munhoz,[38] B. K. Nandi,[14] C. Nattrass,[53] T. K. Nayak,[48] J. M. Nelson,[2] P. K. Netrakanti,[34] M. J. Ng,[4] L. V. Nogach,[33] S. B. Nurushev,[33] G. Odyniec,[22] A. Ogawa,[3] V. Okorokov,[26] E. W. Oldag,[44] D. Olson,[22] M. Pachr,[10] B. S. Page,[15] S. K. Pal,[48] Y. Pandit,[19] Y. Panebratsev,[18] T. Pawlak,[49] T. Peitzmann,[28] V. Perevoztchikov,[3] C. Perkins,[4] W. Peryt,[49] S. C. Phatak,[13] P. Pile,[3] M. Planinic,[54] M. A. Ploskon,[22] J. Pluta,[49] D. Plyku,[30] N. Poljak,[54] A. M. Poskanzer,[22] B. V. K. S. Potukuchi,[17] C. B. Powell,[22] D. Prindle,[50] C. Pruneau,[51] N. K. Pruthi,[31] P. R. Pujahari,[14] J. Putschke,[53] H. Qiu,[21] R. Raniwala,[36] S. Raniwala,[36] R. L. Ray,[44] R. Redwine,[23] R. Reed,[5] H. G. Ritter,[22] J. B. Roberts,[37] O. V. Rogachevskiy,[18] J. L. Romero,[5] A. Rose,[22] C. Roy,[42] L. Ruan,[3] R. Sahoo,[42] S. Sakai,[6] I. Sakrejda,[22] T. Sakuma,[23] S. Salur,[5] J. Sandweiss,[53] E. Sangaline,[5] J. Schambach,[44] R. P. Scharenberg,[34] N. Schmitz,[24] T. R. Schuster,[12] J. Seele,[23] J. Seger,[9] I. Selyuzhenkov,[15] P. Seyboth,[24] E. Shahaliev,[18] M. Shao,[39] M. Sharma,[51] S. S. Shi,[52] E. P. Sichtermann,[22] F. Simon,[24] R. N. Singaraju,[48] M. J. Skoby,[34] N. Smirnov,[53] P. Sorensen,[3] J. Sowinski,[15] H. M. Spinka,[1] B. Srivastava,[34] T. D. S. Stanislaus,[47] D. Staszak,[6] J. R. Stevens,[15] R. Stock,[12] M. Strikhanov,[26] B. Stringfellow,[34] A. A. P. Suaide,[38] M. C. Suarez,[8] N. L. Subba,[19] M. Sumbera,[11] X. M. Sun,[22] Y. Sun,[39] Z. Sun,[21] B. Surrow,[23] D. N. Svirida,[16] T. J. M. Symons,[22] A. Szanto de Toledo,[38] J. Takahashi,[7] A. H. Tang,[3] Z. Tang,[39] L. H. Tarini,[51] T. Tarnowsky,[25] D. Thein,[44] J. H. Thomas,[22] J. Tian,[41] A. R. Timmins,[51] S. Timoshenko,[26] D. Tlusty,[11] M. Tokarev,[18] T. A. Trainor,[50] V. N. Tram,[22] S. Trentalange,[6] R. E. Tribble,[43] O. D. Tsai,[6] J. Ulery,[34] T. Ullrich,[3] D. G. Underwood,[1] G. Van Buren,[3] M. van Leeuwen,[28] G. van Nieuwenhuizen,[23] J. A. Vanfossen Jr.,[19] R. Varma,[14] G. M. S. Vasconcelos,[7] A. N. Vasiliev,[33] F. Videbaek,[3] Y. P. Viyogi,[48] S. Vokal,[18] S. A. Voloshin,[51] M. Wada,[44] M. Walker,[23] F. Wang,[34] G. Wang,[6] H. Wang,[25] J. S. Wang,[21] Q. Wang,[34] X. L. Wang,[39] Y. Wang,[45] G. Webb,[20] J. C. Webb,[3] G. D. Westfall,[25] C. Whitten Jr.,[6] H. Wieman,[22] S. W. Wissink,[15] R. Witt,[46] Y. F. Wu,[52] W. Xie,[34] H. Xu,[21] N. Xu,[22] Q. H. Xu,[40] W. Xu,[6] Y. Xu,[39] Z. Xu,[3] L. Xue,[41] Y. Yang,[21] P. Yepes,[37] K. Yip,[3] I-K. Yoo,[35] Q. Yue,[45] M. Zawisza,[49] H. Zbroszczyk,[49] W. Zhan,[21] J. B. Zhang,[52] S. Zhang,[41] W. M. Zhang,[19] X. P. Zhang,[22] Y. Zhang,[22] Z. P. Zhang,[39] J. Zhao,[41] C. Zhong,[41] J. Zhou,[37] W. Zhou,[40] X. Zhu,[45] Y. H. Zhu,[41] R. Zoulkarneev,[18] and Y. Zoulkarneeva[18]

(STAR Collaboration)

[1]*Argonne National Laboratory, Argonne, Illinois 60439, USA*
[2]*University of Birmingham, Birmingham, United Kingdom*
[3]*Brookhaven National Laboratory, Upton, New York 11973, USA*
[4]*University of California, Berkeley, California 94720, USA*
[5]*University of California, Davis, California 95616, USA*
[6]*University of California, Los Angeles, California 90095, USA*
[7]*Universidade Estadual de Campinas, Sao Paulo, Brazil*
[8]*University of Illinois at Chicago, Chicago, Illinois 60607, USA*

[9]*Creighton University, Omaha, Nebraska 68178, USA*
[10]*Czech Technical University in Prague, FNSPE, Prague, 115 19, Czech Republic*
[11]*Nuclear Physics Institute AS CR, 250 68 Řež/Prague, Czech Republic*
[12]*University of Frankfurt, Frankfurt, Germany*
[13]*Institute of Physics, Bhubaneswar 751005, India*
[14]*Indian Institute of Technology, Mumbai, India*
[15]*Indiana University, Bloomington, Indiana 47408, USA*
[16]*Alikhanov Institute for Theoretical and Experimental Physics, Moscow, Russia*
[17]*University of Jammu, Jammu 180001, India*
[18]*Joint Institute for Nuclear Research, Dubna, 141 980, Russia*
[19]*Kent State University, Kent, Ohio 44242, USA*
[20]*University of Kentucky, Lexington, Kentucky, 40506-0055, USA*
[21]*Institute of Modern Physics, Lanzhou, China*
[22]*Lawrence Berkeley National Laboratory, Berkeley, California 94720, USA*
[23]*Massachusetts Institute of Technology, Cambridge, Massachusetts 02139-4307, USA*
[24]*Max-Planck-Institut für Physik, Munich, Germany*
[25]*Michigan State University, East Lansing, Michigan 48824, USA*
[26]*Moscow Engineering Physics Institute, Moscow, Russia*
[27]*City College of New York, New York City, New York 10031, USA*
[28]*NIKHEF and Utrecht University, Amsterdam, The Netherlands*
[29]*Ohio State University, Columbus, Ohio 43210, USA*
[30]*Old Dominion University, Norfolk, Virginia 23529, USA*
[31]*Panjab University, Chandigarh 160014, India*
[32]*Pennsylvania State University, University Park, Pennsylvania 16802, USA*
[33]*Institute of High Energy Physics, Protvino, Russia*
[34]*Purdue University, West Lafayette, Indiana 47907, USA*
[35]*Pusan National University, Pusan, Republic of Korea*
[36]*University of Rajasthan, Jaipur 302004, India*
[37]*Rice University, Houston, Texas 77251, USA*
[38]*Universidade de Sao Paulo, Sao Paulo, Brazil*
[39]*University of Science & Technology of China, Hefei 230026, China*
[40]*Shandong University, Jinan, Shandong 250100, China*
[41]*Shanghai Institute of Applied Physics, Shanghai 201800, China*
[42]*SUBATECH, Nantes, France*
[43]*Texas A&M University, College Station, Texas 77843, USA*
[44]*University of Texas, Austin, Texas 78712, USA*
[45]*Tsinghua University, Beijing 100084, China*
[46]*United States Naval Academy, Annapolis, Maryland 21402, USA*
[47]*Valparaiso University, Valparaiso, Indiana 46383, USA*
[48]*Variable Energy Cyclotron Centre, Kolkata 700064, India*
[49]*Warsaw University of Technology, Warsaw, Poland*
[50]*University of Washington, Seattle, Washington 98195, USA*
[51]*Wayne State University, Detroit, Michigan 48201, USA*
[52]*Institute of Particle Physics, CCNU (HZNU), Wuhan 430079, China*
[53]*Yale University, New Haven, Connecticut 06520, USA*
[54]*University of Zagreb, Zagreb, HR-10002, Croatia*
(Received 15 March 2011; published 27 June 2011)

The STAR Collaboration at the BNL Relativistic Heavy Ion Collider has measured two-pion correlation functions from $p + p$ collisions at $\sqrt{s} = 200$ GeV. Spatial scales are extracted via a femtoscopic analysis of the correlations, though this analysis is complicated by the presence of strong nonfemtoscopic effects. Our results are put into the context of the world data set of femtoscopy in hadron-hadron collisions. We present the first direct comparison of femtoscopy in $p + p$ and heavy ion collisions, under identical analysis and detector conditions.

DOI: 10.1103/PhysRevC.83.064905 PACS number(s): 25.75.Gz, 25.70.Pq

I. INTRODUCTION AND MOTIVATION

The experimental program of the BNL Relativistic Heavy Ion Collider (RHIC) probes quantum chromodynamics (QCD) from numerous directions. The extraordinary flexibility of the machine permits collisions between heavy and light ions at record energies (up to $\sqrt{s} = 200$ GeV), polarized and unpolarized protons, and strongly asymmetric systems such as $d + \mathrm{Au}$. The proton collisions are the focus of an intense program exploring the spin structure of the nucleon. However, these collisions also serve as a critical "baseline" measurement for the heavy ion physics program that drove the construction of RHIC.

Studies of ultrarelativistic heavy ion collisions aim to explore the equation of state of strongly interacting matter. The highly dynamic nature of the collisions, however, does not allow a purely statistical study of static matter as one might perform in condensed matter physics, but rather requires a detailed understanding of the dynamics itself. If a bulk, self-interacting system is formed (something that should not be assumed *a priori*), the equation of state then plays the dynamic role of generating pressure gradients that drive the collective expansion of the system. Copious evidence [1–4] indicates that a self-interacting system is, in fact, generated in these collisions. The dynamics of the bulk medium is reflected in the transverse momentum (p_T) distribution [5,6] and momentum-space anisotropy (e.g., "elliptic flow") [7,8] of identified particles at low p_T. These observables are well described in a hydrodynamic scenario, in which a nearly perfect (i.e., very low viscosity) fluid expands explosively under the action of pressure gradients induced by the collision [9].

Two-particle femtoscopy [10] (often called "HBT" analysis) measures the space-time substructure of the emitting source at freeze-out, the point at which particles decouple from the system, see, e.g., Ref. [11]. Femtoscopic measurements play a special role in understanding bulk dynamics in heavy ion collisions, for several reasons. First, collective flow generates characteristic space-momentum patterns at freeze-out that are revealed [11] in the momentum dependence of pion "HBT radii" (discussed below), the transverse mass dependence of homogeneity lengths [12], and nonidentical particle correlations [10,13]. Second, while a simultaneous description of particle-identified p_T distributions, elliptic flow, and femtoscopic measurements is easily achieved in flow-dominated toy models (e.g., Ref. [6]), achieving the same level of agreement in a realistic transport calculation is considerably more challenging. In particular, addressing this "HBT puzzle" [14] has led to a deeper understanding of the freeze-out hypersurface, collectivity in the initial stage, and the equation of state. Femtoscopic signals of long dynamical time scales expected for a system undergoing a first-order phase transition [15,16] have not been observed [11], providing early evidence that the system at RHIC evolves from a quark-gluon plasma (QGP) to a hadron gas via a crossover [17]. This sensitive and unique connection to important underlying physics has motivated a huge systematic study of femtoscopic measurements in heavy ion collisions over the past quarter century [11].

HBT correlations from hadron (e.g., $p + p$) and lepton (e.g., $e^+ + e^-$) collisions have been extensively studied in the high-energy physics community as well [18–20], although the theoretical interpretation of the results is less clear and not well developed. Until now, it has been impossible to quantitatively compare femtoscopic results from hadron-hadron collisions to those from heavy ion collisions, due to divergent and often undocumented analysis techniques, detector acceptances, and fitting functions historically used in the high-energy community [20].

In this paper, we exploit the unique opportunity offered by the STAR/RHIC experiment, to make the first direct comparison and quantitative connection between femtoscopy in proton-proton and heavy ion collisions. Systematic complications in comparing these collisions are greatly reduced by using an identical detector and reconstruction software, collision energies, and analysis techniques (e.g., event mixing [21], see below). We observe and discuss the importance of nonfemtoscopic correlations in the analysis of small systems, and put our femtoscopic results for $p + p$ collisions into the context both of heavy ion collisions and (as much as possible) of previous high-energy measurements on hadron-hadron and $e^+ + e^-$ collisions. These results may play a role in understanding the physics behind the space-momentum correlations in these collisions, in the same way that comparison of $p + p$ and heavy ion collision results in the high-p_T sector is crucial to understanding the physics of partonic energy loss [1–4,22]. Our direct comparison also serves as a model and baseline for similar comparisons at higher energies at the CERN Large Hadron Collider (LHC).

We present the analysis of early RHIC $p + p$ runs, taken in 2002 and 2005. Since then, more statistics have been accumulated, the latest with the solenoidal tracker at RHIC (STAR) time-of-flight (TOF) detector [23,24] to extend particle identification capability to higher momentum particles. The analysis of this new data is ongoing. The present results on 2002 and 2005 data already reveal several important points.

The paper is organized as follows. In Sec. II, we discuss the construction of the correlation function and the forms used to parametrize it. Section III discusses details of the analysis, and the results are presented in Sec. IV. In Sec. V, we put these results in the context of previous measurements in $\mathrm{Au} + \mathrm{Au}$ and $p + p(\bar{p})$ collisions. We discuss the similarity between the systematics of HBT radii in heavy ion and particle collisions in Sec. VI and summarize in Sec. VII.

II. TWO-PARTICLE CORRELATION FUNCTION

The two-particle correlation function is generally defined as the ratio of the probability of the simultaneous measurement of two particles with momenta p_1 and p_2, to the product of single-particle probabilities,

$$C(\vec{p}_1, \vec{p}_2) \equiv \frac{P(\vec{p}_1, \vec{p}_2)}{P(\vec{p}_1)P(\vec{p}_2)}. \tag{1}$$

In practice, one usually studies the quantity

$$C_{\vec{p}}(\vec{q}) = \frac{A_{\vec{p}}(\vec{q})}{B_{\vec{p}}(\vec{q})}, \tag{2}$$

where $\vec{q} \equiv \vec{p}_1 - \vec{p}_2$ is the relative momentum. $A(\vec{q})$ is the distribution of the pairs from the same event, and $B(\vec{q})$ is the reference (or "background") distribution. B contains all single-particle effects, including detector acceptance and efficiency, and is usually calculated with an event-mixing technique [11,21]. The explicit label $\vec{P}$ $[\equiv (\vec{p}_1 + \vec{p}_2)/2]$ emphasizes that separate correlation functions are constructed and fitted (see below) as a function of $\vec{q}$, for different selections of the total momentum $\vec{P}$; following convention, we drop the explicit subscript below. Sometimes the measured ratio is normalized to unity at large values of $|\vec{q}|$; we include the normalization in the fit.

In older or statistics-challenged experiments, the correlation function is sometimes constructed in the one-dimensional quantity $Q_{\rm inv} \equiv \sqrt{(\vec{p}_1 - \vec{p}_2)^2 - (E_1 - E_2)^2}$ or two-dimensional variants (see below). More commonly in recent experiments, it is constructed in three dimensions in the so-called out-side-long coordinate system [25–27]. In this system, the "out" direction is that of the pair transverse momentum, the "long" direction is parallel to the beam, and the "side" direction is orthogonal to these two. We will use the subscripts o, l, and s to indicate quantities in these directions.

It has been suggested [28–30] to construct the three-dimensional correlation function using the spherical coordinates

$$q_o = |\vec{q}| \sin\theta \cos\phi, \quad q_s = |\vec{q}| \sin\theta \sin\phi, \quad q_l = |\vec{q}| \cos\theta. \tag{3}$$

This aids in making a direct comparison with the spatial separation distribution through imaging techniques and provides an efficient way to visualize the full three-dimensional structure of $C(\vec{q})$. The more traditional Cartesian projections in the o, s, and l directions integrate over most of the three-dimensional structure, especially at large relative momentum [11,30].

Below, we will present data in the form of the spherical harmonic decomposition coefficients, which depend explicitly on $|\vec{q}|$ as

$$\mathrm{A}_{l,m}(|\vec{q}|) \equiv \frac{1}{\sqrt{4\pi}} \int d\phi \, d(\cos\theta) C(|\vec{q}|, \theta, \phi) Y_{l,m}(\theta, \phi). \tag{4}$$

The coefficient $A_{00}(|\vec{q}|)$ represents the overall angle-integrated strength of the correlation. $A_{20}(|\vec{q}|)$ and $A_{22}(|\vec{q}|)$ are the quadrupole moments of C at a particular value of $|\vec{q}|$. In particular, A_{22} quantifies the second-order oscillation around the long direction; in the simplest HBT analysis, this term reflects nonidentical values of the R_o and R_s HBT radii (see below). Coefficients with odd l represent a dipole moment of the correlation function and correspond to a "shift" in the average position of the first particle in a pair, relative to the second [28–30]. In the present case of identical particles, the labels "first" and "second" become meaningless, and odd-l terms vanish by symmetry. Likewise, for the present case, odd-m terms and all imaginary components vanish as well. See Appendix B of Ref. [30] for a full discussion of symmetries.

In heavy ion collisions, it is usually assumed that all of the correlations between identical pions at low relative momentum are due to femtoscopic effects, i.e., quantum statistics and final-state interactions [11]. At large $|\vec{q}|$, femtoscopic effects vanish [11]. Thus, in the absence of other correlations, $C(\vec{q})$ must approach a constant value independent of the magnitude and direction of $\vec{q}$; equivalently, $A_{l,m}(|\vec{q}|)$ must vanish at large $|\vec{q}|$ for $l \neq 0$.

However, in elementary particle collisions, additional structure at large relative momentum ($|\vec{q}| \gtrsim 400$ MeV/c) has been observed [20,31–35]. Usually this structure is parametrized in terms of a function $\Omega(\vec{q})$ that contributes in addition to the femtoscopic component $C_F(\vec{q})$. Explicitly including the normalization parameter $\mathcal{N}$, then, we will fit our measured correlation functions with the form

$$C(\vec{q}) = \mathcal{N} \, C_F(\vec{q}) \, \Omega(\vec{q}). \tag{5}$$

Below, we discuss separately various parametrizations of the femtoscopic and nonfemtoscopic components, which we use in order to connect with previous measurements. A historical discussion of these forms may be found in Ref. [20].

We use a maximum-likelihood fit to the correlation functions, though chi-square minimization yields almost identical results, and we give the χ^2 values for all fits below. As we shall see, none of the functional forms perfectly fit the data. However, the characteristic scales of the source can be extracted and compared with identical fits to previous data.

A. Femtoscopic correlations

Femtoscopic correlations between identical pions are dominated by Bose-Einstein symmetrization and Coulomb final-state effects in the two-pion wave function [11].

In all parametrizations, the overall strength of the femtoscopic correlation is characterized by a parameter λ [11]. Historically called the "chaoticity" parameter, it generally accounts for particle identification efficiency, long-lived decays, and long-range tails in the separation distribution [36].

In the simplest case, the Bose-Einstein correlations are often parametrized by a Gaussian,

$$C_F(Q_{\rm inv}) = 1 + \lambda e^{-Q_{\rm inv}^2 R_{\rm inv}^2}, \tag{6}$$

where $R_{\rm inv}$ is a one-dimensional HBT radius.

Kopylov and Podgoretskii [37] introduced an alternative, two-dimensional parametrization

$$C_F(q_T, q_0) = 1 + \lambda \left[\frac{2J_1(q_T R_B)}{q_T R_B} \right]^2 \left(1 + q_0^2 \tau^2\right)^{-1}, \tag{7}$$

where q_T is the component of $\vec{q}$ orthogonal to $\vec{P}$, $q_0 = E_1 - E_2$, R_B and τ are the size and decay constants of a spherical emitting source, and J_1 is the first-order Bessel function. This is similar to another common historical parametrization (e.g., Ref. [38]) characterizing the source with a spatial and temporal scale

$$C_F(q, q_0) = 1 + \lambda e^{-q_T^2 R_G^2 - q_0^2 \tau^2}. \tag{8}$$

Simple numerical studies show that R_G from Eq. (8) is approximately half as large as R_B obtained from Eq. (7) [20,38,39].

With sufficient statistics, a three-dimensional correlation function may be measured. We calculate the relative

momentum in the longitudinally comoving system (LCMS), in which the total longitudinal momentum of the pair, $p_{l,1}+p_{l,2}$, vanishes [40]. For heavy ion and hadron-hadron collisions, this "longitudinal" direction $\hat{l}$ is taken to be the beam axis [11]; for $e^+ + e^-$ collisions, the thrust axis is used.

For a Gaussian emission source, femtoscopic correlations due only to Bose-Einstein symmetrization are given by [11]

$$C_F(q_o, q_s, q_l) = 1 + \lambda e^{-q_o^2 R_o^2 - q_s^2 R_s^2 - q_l^2 R_l^2}, \tag{9}$$

where R_o, R_s, and R_l are the spatial scales of the source.

While older papers sometimes ignored the Coulomb final-state interaction between the charged pions [20], it is usually included by using the Bowler-Sinyukov [41,42] functional form

$$C_F(Q_{\rm inv}) = (1-\lambda) + \lambda K_{\rm coul}(Q_{\rm inv})\left(1 + e^{-Q_{\rm inv}^2 R_{\rm inv}^2}\right), \tag{10}$$

and in three dimensions,

$$C_F(q_o, q_s, q_l) = (1-\lambda) + \lambda K_{\rm coul}(Q_{\rm inv})\left(1 + e^{-q_o^2 R_o^2 - q_s^2 R_s^2 - q_l^2 R_l^2}\right). \tag{11}$$

Here, $K_{\rm coul}$ is the squared Coulomb wave function integrated over the source emission points and over the angles of the relative momentum vector in the pair rest frame.

B. Nonfemtoscopic correlations

In the absence of nonfemtoscopic effects, one of the forms for $C_F(\vec{q})$ from Sec. II A is fitted to the measured correlation function; i.e., $\Omega = 1$ in Eq. (5). Such a "standard fit" works well in the high-multiplicity environment of heavy ion collisions [11]. In hadron-hadron or $e^+ + e^-$ collisions, however, it does not describe the measured correlation function well, especially as $|q|$ increases. Most authors attribute the nonfemtoscopic structure to momentum conservation effects in these small systems. While this large-$|q|$ behavior is sometimes simply ignored, it is usually included in the fit either through *ad hoc* [32] or physically motivated [30] terms.

In this paper, we will use three selected parametrizations of the nonfemtoscopic correlations and study their effects on the femtoscopic parameters obtained from the fit to experimental correlation functions. The first formula assumes that the nonfemtoscopic contribution can be parametrized by a first-order polynomial in $\vec{q}$ components (used e.g., in Refs. [43–47]). Respectively, the one- and three-dimensional forms used in the literature are

$$\Omega(q) = 1 + \delta q, \tag{12}$$

and

$$\Omega(\vec{q}) = \Omega(q_o, q_s, q_l) = 1 + \delta_o q_o + \delta_s q_s + \delta_l q_l. \tag{13}$$

For simplicity, we will use the name "δ-q fit" when we fit Eq. (12) or (13) to one- or three-dimensional correlation functions.

The ALICE Collaboration [48] uses a second-order polynomial to parametrize the nonfemtoscopic correlations in one-dimensional correlation functions,

$$\Omega(q) = 1 + bq + cq^2. \tag{14}$$

We will use this to compare with the data in Sec. IV B.

Another form [49] assumes that nonfemtoscopic correlations contribute $|\vec{q}|$-independent values to the $l = 2$ moments in Eq. (4). In terms of the fitting parameters ζ and β,

$$\begin{aligned}\Omega(|\vec{q}|, \cos\theta, \phi) &= \Omega(\cos\theta, \phi) \\ &= 1 + 2\sqrt{\pi}\{\beta Y_{2,0}(\cos\theta, \phi) + 2\zeta \,\mathrm{Re}[Y_{2,2}(\cos\theta, \phi)]\} = 1 \\ &\quad + \beta\sqrt{\frac{5}{4}}(3\cos^2\theta - 1) + \zeta\sqrt{\frac{15}{2}}\sin^2\theta\cos 2\phi.\end{aligned} \tag{15}$$

For simplicity, fits using this form for the nonfemtoscopic effects will be referred to as "ζ-β fits."

These two forms (as well as others that can be found in the literature [20]) are purely empirical, motivated essentially by the shape of the observed correlation function itself. While most authors attribute these effects primarily to momentum conservation in these low-multiplicity systems, the parameters and functional forms themselves cannot be directly connected to this or any physical mechanism. One may identify two dangers of using an *ad hoc* form to quantify nonfemtoscopic contributions to $C(\vec{q})$. First, while they describe (by construction) the correlation function well at large $|\vec{q}|$, for which femtoscopic contributions vanish, there is no way to constrain their behavior at low $|\vec{q}|$ where both femtoscopic and (presumably) nonfemtoscopic correlations exist. Even simple effects like momentum conservation give rise to nonfemtoscopic correlations that vary nontrivially even at low $|\vec{q}|$. Misrepresenting the nonfemtoscopic contribution in $\Omega(\vec{q})$ can therefore distort the femtoscopic radius parameters in $C_F(\vec{q})$, especially considering the small radius values in $p+p$ collisions. Second, there is no way to estimate whether the best-fit parameter values in an *ad hoc* functional form are physically "reasonable."

If the nonfemtoscopic correlations are in fact dominated by energy and momentum conservation, as is usually supposed, one may derive an analytic functional form for Ω. In particular, the multiparticle phase-space constraints for a system of N particles project onto the two-particle space as [30]

$$\begin{aligned}\Omega(p_1, p_2) = 1 &- M_1\,\overline{\{\vec{p}_{1,T}\cdot\vec{p}_{2,T}\}} - M_2\,\overline{\{p_{1,z}\,p_{2,z}\}} \\ &- M_3\,\overline{\{E_1\,E_2\}} + M_4\,\overline{\{E_1 + E_2\}} - \frac{M_4^2}{M_3},\end{aligned} \tag{16}$$

where

$$\begin{aligned}M_1 &\equiv \frac{2}{N\langle p_T^2\rangle}, \quad M_2 \equiv \frac{1}{N\langle p_z^2\rangle} \\ M_3 &\equiv \frac{1}{N(\langle E^2\rangle - \langle E\rangle^2)}, \quad M_4 \equiv \frac{\langle E\rangle}{N(\langle E^2\rangle - \langle E\rangle^2)}.\end{aligned} \tag{17}$$

The notation $\overline{\{X\}}$ in Eq. (16) is used to indicate that X is the average of a two-particle quantity which depends on p_1 and p_2 (or $\vec{q}$, etc.). In particular,

$$\overline{\{X\}}(\vec{q}) \equiv \frac{\int d^3\vec{p}_1 \int d^3\vec{p}_2 P(\vec{p}_1)P(\vec{p}_2)X\delta\mathbf{(}\vec{q} - (\vec{p}_1 - \vec{p}_2)\mathbf{)}}{\int d^3\vec{p}_1 \int d^3\vec{p}_2 P(\vec{p}_1)P(\vec{p}_2)\delta\mathbf{(}\vec{q} - (\vec{p}_1 - \vec{p}_2)\mathbf{)}}, \tag{18}$$

where P represents the single-particle probability first seen in Eq. (1).

In practice, this means generating histograms in addition to $A(\vec{q})$ and $B(\vec{q})$ [cf. Eq. (2)] as one loops over mixed pairs of particles i and j in the data analysis. For example,

$$\overline{\{\vec{p}_{1,T}\cdot\vec{p}_{2,T}\}}(\vec{q}) = \frac{\left(\sum_{i,j}\vec{p}_{i,T}\cdot\vec{p}_{j,T}\right)(\vec{q})}{B(\vec{q})}, \tag{19}$$

where the sum in the numerator runs over all pairs in all events.

In Eq. (16), the four fit parameters M_i are directly related to five physical quantities (the number of particles N, $\langle p_T^2\rangle$, $\langle p_z^2\rangle$, $\langle E^2\rangle$, and $\langle E\rangle$) through Eq. (17). Assuming that

$$\langle E^2\rangle \approx \langle p_T^2\rangle + \langle p_z^2\rangle + m_*^2, \tag{20}$$

where m_* is the mass of a typical particle in the system (for our pion-dominated system, $m_* \approx m_\pi$), then one may solve for the physical parameters. For example,

$$N \approx \frac{M_1^{-1} + M_2^{-1} - M_3^{-1}}{\left(\frac{M_4}{M_3}\right)^2 - m_*^2}. \tag{21}$$

Since we cannot know exactly the values of $\langle E^2\rangle$, etc., that characterize the underlying distribution in these collisions, we treat the M_i as free parameters in our fits, and then consider whether their values are mutually compatible and physical. For a more complete discussion, see Refs. [30,50].

In Ref. [30], the correlations leading to Eq. (16) were called "EMCICs" (short for energy and momentum conservation-induced correlations); we will refer to fits using this function with this acronym in our figures.

C. Parameter counting

As mentioned, we will be employing a number of different fitting functions, each of which contains several parameters. It is appropriate at this point to briefly take stock.

In essentially all modern HBT analyses, on the order of five to six parameters quantify the femtoscopic correlations. For the common Gaussian fit [Eq. (11)], one has three HBT radii, the chaoticity parameter, and the normalization $\mathcal{N}$. Recent "imaging" fits approximate the two-particle emission zone as a sum of spline functions, the weights of which are the parameters [51]; the number of splines (hence weights) used is $\sim$5. Other fits (e.g., double Gaussian and exponential-plus-Gaussian) [18,52] contain a similar number of femtoscopic parameters. In all cases, a distinct set of parameters is extracted for each selection of $\vec{P}$ [see Eq. (2) and surrounding discussion].

Accounting for the nonfemtoscopic correlations inevitably increases the total number of fit parameters. The ζ-β functional form [Eq. (15)] involves two parameters, the δ-q form [Eq. (13)] three, and the EMCIC form [Eq. (16)] four. However, it is important to keep in mind that using the ζ-β (δ-q) form means two (three) additional parameters *for each selection* of $\vec{P}$ when forming the correlation functions. On the other hand, the four EMCIC parameters cannot depend on $\vec{P}$. Therefore, when fitting $C_{\vec{P}}(\vec{q})$ for four selections of $\vec{P}$, use of the ζ-β, δ-q, and EMCIC forms increases the total number of parameters by 8, 12, and 4, respectively.

III. ANALYSIS DETAILS

Our results are based on $p+p$ collisions measured by STAR in the 2002 and 2005 runs at RHIC. As mentioned in Sec. I, there is significant advantage in analyzing $p+p$ collisions in the same way that heavy ion collisions are analyzed. Therefore, the results discussed in this paper are produced with the same techniques and acceptance cuts as have been used for previous pion femtoscopy studies by STAR [53–56]. Here we discuss some of the main points; full systematic studies of cuts and techniques can be found in Ref. [55].

The primary subdetector used in this analysis to reconstruct particles is the time projection chamber (TPC) [57]. Pions could be identified up to a momentum of 800 MeV/c by correlating their momentum and specific ionization loss (dE/dx) in the TPC gas. A particle was considered to be a pion if its dE/dx value for a given momentum was within two sigma of the Bichsel expectation [58] (an improvement on the Bethe-Bloch formula [59] for thin materials) for a pion, and more than two sigma from the expectations for electrons, kaons, and protons. By varying the cuts on energy loss to allow more or less contamination from kaons or electrons, we estimate that impurities in the pion sample lead to an uncertainty in the femtoscopic scale parameters (e.g., HBT radii) of only about 1%. Particles were considered for analysis if their reconstructed tracks produced hits on at least 10 of the 45 padrows, and their distance of closest approach (DCA) to the primary vertex was less than 3 cm. The lower momentum cut of 120 MeV/c is imposed by the TPC acceptance and the magnetic field. Only tracks at midrapidity ($|y| < 0.5$) were included in the femtoscopic analysis.

Events were recorded based on a coincidence trigger of two beam-beam counters (BBCs), annular scintillator detectors located $\pm$3.5 m from the interaction region and covering the pseudorapidity range $3.3 < |\eta| < 5.0$. Events were selected for analysis if the primary collision vertex was within 30 cm of the center of the TPC. The further requirement that events include at least two like-sign pions increases the average charged-particle multiplicity with $|\eta| < 0.5$ from 3.0 (without the requirement) to 4.25. Since particle *pairs* enter into the correlation function, the effective average multiplicity is higher; in particular, the pair-weighted charged-particle multiplicity at midrapidity is about 6.0. After event cuts, about 5×10^6 minimum-bias events from $p+p$ collisions at $\sqrt{s} = 200$ GeV were used. A higher statistics analysis of $p+p$ collisions measured in 2007 and 2009 is underway. With greater statistics, the strong femtoscopic and nonfemtoscopic structures we present in the current analysis will be studied with higher precision.

Two-track effects, such as splitting (one particle reconstructed as two tracks) and merging (two particles reconstructed as one track) were treated identically as has been done in STAR analyses of Au + Au collisions [55]. Both effects can affect the shape of $C(\vec{q})$ at very low $|\vec{q}| \lesssim 20$ MeV/c, regardless of the colliding system. However, their effect on the extracted sizes in $p+p$ collisions turns out to be smaller than statistical errors, because small ($\sim$1 fm) sources lead to large ($\sim$200 MeV/c) femtoscopic structures in the correlation function.

The analysis presented in this paper was done for four bins in average transverse momentum k_T [$\equiv \frac{1}{2}|(\vec{p}_{T,1}+\vec{p}_{T,2})|$]: 150–250, 250–350, 350–450, and 450–600 MeV/c. The systematic errors on femtoscopic radii due to the fit range, particle misidentification, two-track effects, and the Coulomb radius [used to calculate $K_{\rm coul}$ in Eqs. (10) and (11)] are estimated to be about 10%, similar to previous studies [55].

IV. RESULTS

In this section, we present the correlation functions and fits to them, using the various functional forms discussed in Sec. II. The m_T and multiplicity dependence of femtoscopic radii from these fits are compared here and put into the broader context of data from heavy ion and particle collisions in the next section.

Figure 1 shows the two-pion correlation function for minimum-bias $p+p$ collisions for $0.35 < k_T < 0.45$ GeV/c. The three-dimensional data are represented with the traditional one-dimensional Cartesian projections [11]. For the projection on q_o, integration in q_s and q_l was done over the range

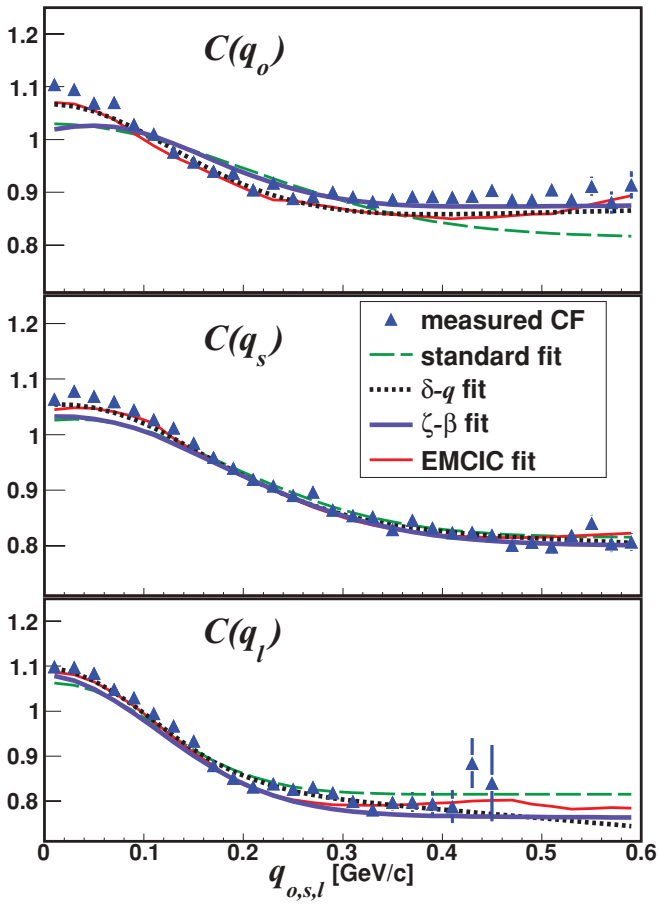

FIG. 1. (Color online) Cartesian projections of the 3D correlation function from $p+p$ collisions at $\sqrt{s}=200$ GeV for $k_T=[0.35, 0.45]$ GeV/c (blue triangles). Femtoscopic effects are parametrized with the form in Eq. (11); different curves represent various parametrizations of nonfemtoscopic correlations used in the fit and described in detail in Sec. II B.

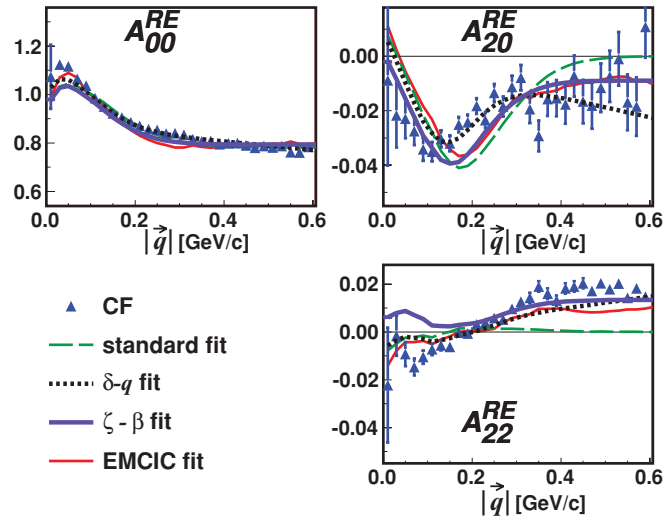

FIG. 2. (Color online) First three nonvanishing moments of the spherical harmonic decomposition of the correlation function from $p+p$ collisions at $\sqrt{s}=200$ GeV, for $k_T=[0.15, 0.25]$ GeV/c. Femtoscopic effects are parametrized with the form in Eq. (11); different curves represent various parametrizations of nonfemtoscopic correlations used in the fit and described in detail in Sec. II B. The superscript RE in $A^{\rm RE}_{l,m}$ stands for the real part of $A_{l,m}$.

[0.00, 0.12] GeV/c. As discussed in Sec. II and in more detail in Ref. [30], the full structure of the correlation function is best seen in the spherical harmonic decomposition, shown in Figs. 2–5.

In what follows, we discuss systematics of fits to the correlation function, with particular attention to the femtoscopic parameters. It is important to keep in mind that the fits are performed on the full three-dimensional correlation function $C(\vec{q})$. The choice to plot the data and fits as spherical harmonic coefficients A_{lm} or as Cartesian projections along the out, side, and long directions is based on the desire to present results in the traditional format (projections) or in a representation more sensitive to the three-dimensional structure of the data [30]. In

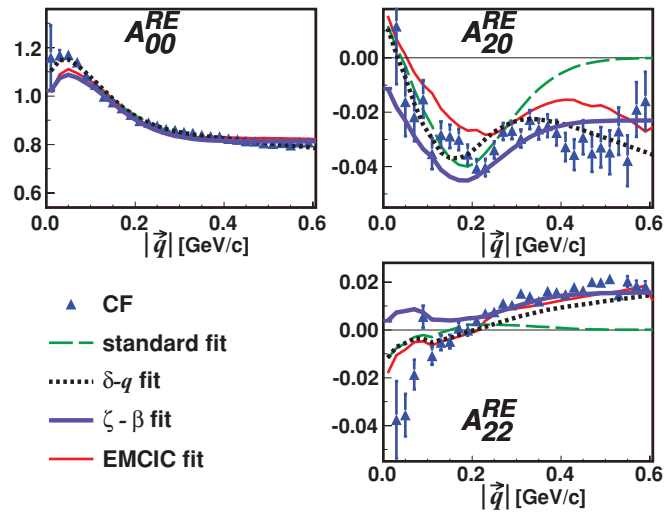

FIG. 3. (Color online) As for Fig. 2, but for $k_T=[0.25, 0.35]$ GeV/c.

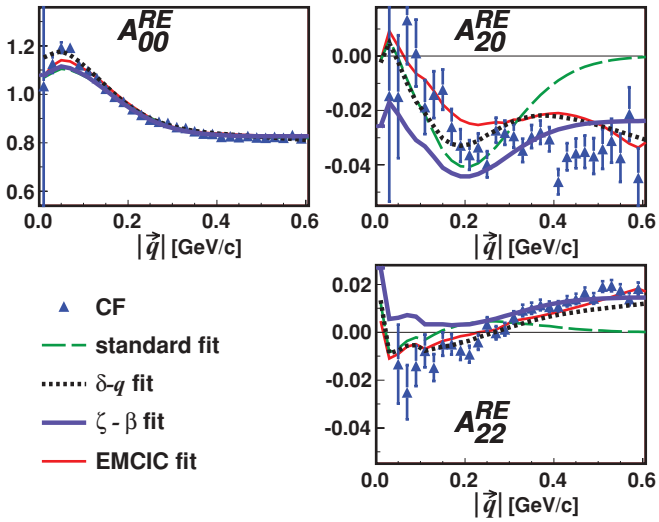

FIG. 4. (Color online) As for Fig. 2, but for $k_T = [0.35, 0.45]$ GeV/c.

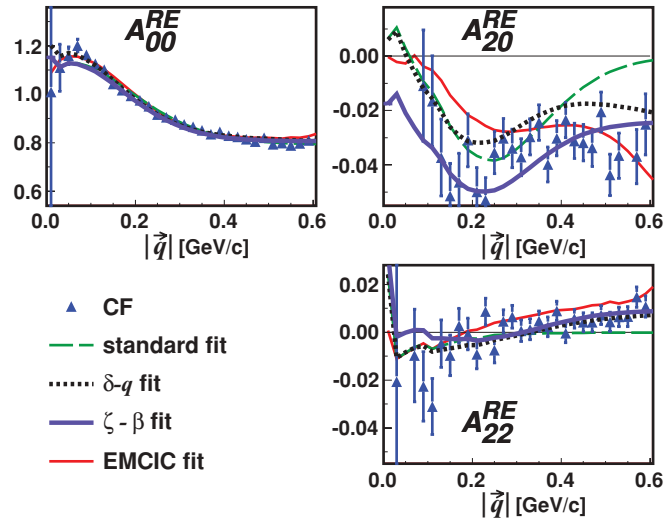

FIG. 5. (Color online) As for Fig. 2, but for $k_T = [0.45, 0.60]$ GeV/c.

particular, the data and fits shown in Fig. 1, for $k_T = 0.35$–0.45 GeV/c, are the same as those shown in Fig. 4.

A. Transverse mass dependence of 3D femtoscopic radii

Femtoscopic scales from three-dimensional (3D) correlation functions are usually extracted by fitting to the functional form given in Eq. (11). To make a connection to previous measurements, we employ the same form and vary the treatment of nonfemtoscopic effects as discussed in Sec. II B. The fits are shown as curves in Figs. 1–5; the slightly fluctuating structure observable in the sensitive spherical harmonic representation in Figs. 2–5 results from finite-binning effects in plotting [60].

Dashed green curves in Figs. 1–5 represent the "standard fit," in which nonfemtoscopic correlations are neglected altogether ($\Omega = 1$). Black dotted and purple dashed curves, respectively, indicate δ-q [Eq. (13)] and ζ-β [Eq. (15)] forms. Solid red curves represent fits in which the nonfemtoscopic contributions follow the EMCIC [Eq. (16)] form. None of the functional forms perfectly fit the experimental correlation function, though the nonfemtoscopic structure is semiquantitatively reproduced by the *ad hoc* δ-q and ζ-β fits (by construction) and the EMCIC fit (nontrivially). Rather than invent yet another *ad hoc* functional form to better fit the data, we will consider the radii produced by all of these forms.

The fit parameters for these four fits and for each of the four k_T bins are given in Tables I–IV. Considering first the nonfemtoscopic correlations, we observe that the *ad hoc* fit parameters $\delta_{o,s,l}$ in Table II and ζ and β in Table III are different for each k_T bin. Due to their physical meaning, the EMCIC parameters M_{1-4} are fixed for all k_T values, as indicated in Table IV. Setting the characteristic particle mass to that of the pion and using Eqs. (17), (20), and (21), the nonfemtoscopic parameters listed in Table IV correspond to the following values characteristic of the emitting system:

$$\begin{aligned} N &= 14.3 \pm 4.7, \\ \langle p_T^2 \rangle &= 0.17 \pm 0.06\ (\mathrm{GeV}/c)^2, \\ \langle p_z^2 \rangle &= 0.32 \pm 0.13\ (\mathrm{GeV}/c)^2, \\ \langle E^2 \rangle &= 0.51 \pm 0.11\ \mathrm{GeV}^2, \\ \langle E \rangle &= 0.68 \pm 0.08\ \mathrm{GeV}. \end{aligned}$$

These values are rather reasonable [50].

HBT radii from the different fits are plotted as a function of transverse mass in Fig. 6. The treatment of the nonfemtoscopic correlations significantly affects the magnitude of the femtoscopic length scales extracted from the fit, especially in the out and long directions, for which variations up to 50% in magnitude are observed. The dependence of the radii on $m_T \equiv \sqrt{k_T^2 + m^2}$ is quite similar in all cases. We discuss this dependence further in Sec. V.

TABLE I. Results from a fit to data from $p + p$ collisions at $\sqrt{s}$= 200 GeV using Eq. (11) to parametrize the femtoscopic correlations ("standard fit").

k_T (GeV/c)	R_o (fm)	R_s (fm)	R_l (fm)	λ	χ^2/ndf
[0.15, 0.25]	0.84 ± 0.02	0.89 ± 0.01	1.53 ± 0.02	0.422 ± 0.004	2012 / 85
[0.25, 0.35]	0.81 ± 0.02	0.88 ± 0.01	1.45 ± 0.02	0.422 ± 0.005	1852 / 85
[0.35, 0.45]	0.71 ± 0.02	0.82 ± 0.02	1.31 ± 0.02	0.433 ± 0.007	941 / 85
[0.45, 0.60]	0.68 ± 0.02	0.68 ± 0.01	1.05 ± 0.02	0.515 ± 0.009	278 / 85

TABLE II. Results from a fit to data from $p+p$ collisions at $\sqrt{s}$= 200 GeV using Eq. (11) to parametrize the femtoscopic correlations and Eq. (13) for nonfemtoscopic ones ("δ-q fit").

k_T (GeV/c)	R_o (fm)	R_s (fm)	R_l (fm)	λ	δ_o	δ_s	δ_l	χ^2/ndf
[0.15, 0.25]	1.30 ± 0.03	1.05 ± 0.03	1.92 ± 0.05	0.295 ± 0.004	0.0027 ± 0.0026	-0.1673 ± 0.0052	-0.2327 ± 0.0078	471 / 82
[0.25, 0.35]	1.21 ± 0.03	1.05 ± 0.03	1.67 ± 0.05	0.381 ± 0.005	0.0201 ± 0.0054	-0.1422 ± 0.0051	-0.2949 ± 0.0081	261 / 82
[0.35, 0.45]	1.10 ± 0.03	0.94 ± 0.03	1.37 ± 0.05	0.433 ± 0.007	0.0457 ± 0.0059	-0.0902 ± 0.0053	-0.2273 ± 0.0090	251 / 82
[0.45, 0.60]	0.93 ± 0.03	0.82 ± 0.03	1.17 ± 0.05	0.480 ± 0.009	0.0404 ± 0.0085	-0.0476 ± 0.0093	-0.1469 ± 0.0104	189 / 82

B. Transverse mass dependence of 1D femtoscopic radii

Since three-dimensional correlation functions encode more information about the homogeneity region than do one-dimensional (1D) correlation functions, they are also more statistics hungry. Therefore, most previous particle physics experiments have constructed and analyzed the latter. For the sake of making the connection between our results and existing world systematics, we perform similar analyses as those found in the literature.

The first important connection to make is for the m_T dependence of HBT radii from minimum-bias $p+p$ collisions. We extract the one-dimensional HBT radius $R_{\rm inv}$ associated with the femtoscopic form in Eq. (10), using three forms for the nonfemtoscopic terms. For four selections in k_T, Table V lists the fit parameters for the "standard" fit that neglects nonfemtoscopic correlations altogether ($\Omega = 1$). Tables VI and VII list results when using the 1D δ-q form [Eq. (12)] and the EMCIC form [Eq. (16)], respectively. In performing the EMCIC fit, the nonfemtoscopic parameters M_{1-4} were kept fixed at the values listed in Table IV. The one-dimensional radii from the three different treatments of nonfemtoscopic effects are plotted as a function of m_T in Fig. 9. The magnitude of the radius using the *ad hoc* δ-q fit is $\sim 25\%$ larger than that from either the standard or EMCIC fit, but again all show similar dependence on m_T.

To complete the study of nonfemtoscopic treatments, we apply the prescription developed by the ALICE Collaboration [48] for one-dimensional correlation functions in $q_{\rm inv}$. In particular, minimum-bias events generated with the PYTHIA event generator [61] v6.319 have been filtered through the analysis cuts. The model parameters were set according to the Collider Detector at Fermilab (CDF) Tune A settings [63,64] which are used to study the underlying event in $p+p$ collisions at STAR [65]. To simulate tracking resolution effects, particle momentum was smeared by about 2%, such that the experimentally measured $K^0_S \to \pi^+\pi^-$ peak was reproduced. By way of a cross-check, we compare measured and PYTHIA-generated correlation functions for oppositely signed pions; these are shown in Fig. 7, for four selections of k_T. Since the model does not include final-state Coulomb effects, the peak at low $q_{\rm inv}$ seen in the data is not reproduced. Nonfemtoscopic structures at large $q_{\rm inv}$ are relatively well reproduced, except for the lowest k_T selection, in which they are overpredicted. Both in the data and in the model, these structures are significantly less pronounced than those seen in $\sqrt{s_{NN}} = 900$ GeV collisions at the LHC [48].

The dominant nonfemtoscopic structures seen by the ALICE Collaboration at the LHC are likely due to hard partonic processes. We found that requiring the high-p_T scattering processes ($35 < \hat{p_T} < 45$ GeV/c) in the PYTHIA model for $\sqrt{s_{NN}} = 200$ GeV collisions generates nonfemtoscopic structures of the similar magnitude as those measured by the ALICE Collaboration at $\sqrt{s_{NN}} = 900$ GeV; such a requirement biases the event collection toward hard processes and increases the event multiplicity. Similarly, in PYTHIA simulations at both energies, selection of high-multiplicity events yields stronger nonfemtoscopic structures [62]. Not surprisingly, contributions from hard processes in minimum-bias collisions at $\sqrt{s_{NN}} = 200$ GeV are much smaller than high-multiplicity collisions at the LHC.

In Figure 8, we plot the measured and PYTHIA-simulated correlation functions for like-sign pions. Again, the peak at low $q_{\rm inv}$ is not reproduced by the model, since it does not include Bose-Einstein effects. Following the procedure of the ALICE Collaboration [48], we fit the PYTHIA-generated correlation function with a second-order polynomial in $q_{\rm inv}$ [Eq. (14)]. The experimental correlation function is then fit using Eq. (10) for the femtoscopic correlations and Eq. (14) for the nonfemtoscopic ones, keeping the parameters b and c fixed from the fit to the PYTHIA-generated correlations (open symbols in Fig. 8). The results are given in Table VIII and shown as open circles in Fig. 9. The m_T dependence of the HBT radii persists when using this procedure.

TABLE III. Results from a fit to data from $p+p$ collisions at $\sqrt{s}$= 200 GeV using Eq. (11) to parametrize the femtoscopic correlations and Eq. (15) for nonfemtoscopic ones ("ζ-β fit").

k_T (GeV/c)	R_o (fm)	R_s (fm)	R_l (fm)	λ	ζ	β	χ^2/ndf
[0.15, 0.25]	1.24 ± 0.04	0.92 ± 0.03	1.71 ± 0.04	0.392 ± 0.008	0.0169 ± 0.0021	-0.0113 ± 0.0019	1720 / 83
[0.25, 0.35]	1.14 ± 0.05	0.89 ± 0.04	1.37 ± 0.08	0.378 ± 0.006	0.0193 ± 0.0034	-0.0284 ± 0.0031	823 / 83
[0.35, 0.45]	1.02 ± 0.04	0.81 ± 0.05	1.20 ± 0.07	0.434 ± 0.008	0.0178 ± 0.0029	-0.0289 ± 0.0032	313 / 83
[0.45, 0.60]	0.89 ± 0.04	0.71 ± 0.05	1.09 ± 0.06	0.492 ± 0.009	0.0114 ± 0.0023	-0.0301 ± 0.0041	190 / 83

TABLE IV. Results from a fit to data from $p + p$ collisions at $\sqrt{s}$= 200 GeV using Eq. (11) to parametrize the femtoscopic correlations and Eq. (16) for nonfemtoscopic ones ("EMCIC fit").

k_T (GeV/c)	R_o (fm)	R_s (fm)	R_l (fm)	λ	M_1 [(GeV/c)$^{-2}$]	M_2 [(GeV/c)$^{-2}$]	M_3 (GeV^{-2})	M_4 (GeV^{-1})	χ^2/ndf
[0.15, 0.25]	1.06 ± 0.03	1.00 ± 0.04	1.38 ± 0.05	0.665 ± 0.005					
[0.25, 0.35]	0.96 ± 0.02	0.95 ± 0.03	1.21 ± 0.03	0.588 ± 0.006	0.43 ± 0.07	0.22 ± 0.06	1.51 ± 0.12	1.02 ± 0.09	2218 / 336
[0.35, 0.45]	0.89 ± 0.02	0.88 ± 0.02	1.08 ± 0.04	0.579 ± 0.009					
[0.45, 0.60]	0.78 ± 0.04	0.79 ± 0.02	0.94 ± 0.03	0.671 ± 0.028					

C. Multiplicity dependence of 1D femtoscopic radii

To compare with the multiplicity dependence of k_T-integrated HBT radii reported in high-energy particle collisions, we combine k_T bins and separately analyze low ($dN_{\rm ch}/d\eta \leqslant 6$) and high ($dN_{\rm ch}/d\eta \geqslant 7$) multiplicity events. The choice of the cut was dictated by the requirement of sufficient pair statistics in the two event classes. Fit parameters for common fitting functions are given in Table IX for minimum-bias and multiplicity-selected collisions.

Figure 10 shows the multiplicity dependence of the common one-dimensional HBT radius $R_{\rm inv}$, extracted by parametrizing the femtoscopic correlations according to Eq. (10). Nonfemtoscopic effects were either ignored (standard fit $\Omega = 1$) or parametrized with the δ-q [Eq. (12)] or EMCIC [Eq. (16)] functional form. To keep the parameter count down, the EMCIC kinematic parameters ($\langle p_T^2 \rangle$, $\langle p_z^2 \rangle$, $\langle E^2 \rangle$, $\langle E \rangle$) were kept fixed to the values obtained from the 3D fit, and only N was allowed to vary. In all cases, $R_{\rm inv}$ is observed to increase with multiplicity. Parametrizing nonfemtoscopic effects according to the EMCIC form gives results similar to those of a standard fit ignoring them, whereas the δ-q form generates an offset of approximately 0.3 fm, similar to all three- and one-dimensional fits discussed above. That different numerical values are obtained for somewhat different fitting functions is not surprising. The point we focus on is that the systematic dependences of the femtoscopic scales, with both k_T and multiplicity, are robust.

Table X lists fit parameters to two-dimensional correlation functions in q_T and q_0, using Eqs. (7) and (8). The radius from the former fit is approximately twice that of the latter, as expected (see Sec. II A). These values will be compared with previously measured data in the next section.

TABLE V. Results from a fit to the 1D correlation function from $p + p$ collisions at $\sqrt{s} = 200$ GeV using Eq. (6) to parametrize the femtoscopic correlations (standard fit).

k_T (GeV/c)	$R_{\rm inv}$ (fm)	λ	χ^2/ndf
[0.15, 0.25]	1.32 ± 0.02	0.345 ± 0.005	265/27
[0.25, 0.35]	1.26 ± 0.02	0.357 ± 0.007	203/27
[0.35, 0.45]	1.18 ± 0.02	0.348 ± 0.008	243/27
[0.45, 0.60]	1.05 ± 0.03	0.413 ± 0.012	222/27

V. COMPARISON WITH WORLD SYSTEMATICS

In this section, we make the connection between femtoscopic measurements in heavy ion collisions and those in particle physics by placing our results in the context of world systematics from each.

A. Results in the context of heavy ion systematics

The present measurements represent the first opportunity to study femtoscopic correlations from hadronic collisions and heavy ion collisions, using the same detector, reconstruction, analysis, and fitting techniques. The comparison should be direct, and differences in the extracted HBT radii should arise from differences in the source geometry itself. In fact, especially in recent years, the heavy ion community has generally arrived at a consensus among the different experiments regarding the analysis techniques, fitting functions, and reference frames to use. This, together with good documentation of event selection and acceptance cuts, has led to a quantitatively consistent world systematics of femtoscopic measurements in heavy ion collisions over two orders of magnitude in collision energy [11]; indeed, at RHIC, the

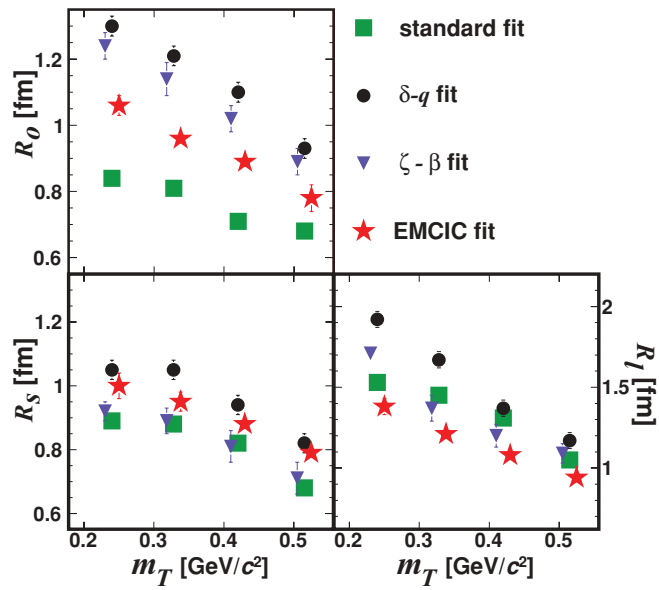

FIG. 6. (Color online) m_T dependence of the 3D femtoscopic radii in $p + p$ collisions at $\sqrt{s} = 200$ GeV for different parametrizations of the nonfemtoscopic correlations. See text for more details. Data have been shifted slightly in the abscissa for clarity.

TABLE VI. Results from a fit to the 1D correlation function from $p+p$ collisions at $\sqrt{s}=200$ GeV using Eq. (6) to parametrize the femtoscopic correlations and Eq. (12) for nonfemtoscopic ones (δ-q fit).

k_T (GeV/c)	$R_{\rm inv}$ (fm)	λ	δ	χ^2/ndf
[0.15, 0.25]	1.72 ± 0.04	0.285 ± 0.007	-0.237 ± 0.007	86/26
[0.25, 0.35]	1.65 ± 0.04	0.339 ± 0.009	-0.163 ± 0.008	80/26
[0.35, 0.45]	1.49 ± 0.05	0.308 ± 0.011	-0.180 ± 0.015	71/26
[0.45, 0.60]	1.41 ± 0.06	0.338 ± 0.016	-0.228 ± 0.017	78/26

agreement in HBT radii from the different experiments is remarkably good. Thus, inasmuch as STAR's measurement of HBT radii from $p+p$ collisions may be directly compared with STAR's HBT radii from Au + Au collisions, they may be equally well compared with the world's systematics of all heavy ion collisions.

As with most heavy ion observables at low transverse momentum [66], the HBT radii R_s and R_l scale primarily with event multiplicity [11] (or, at lower energies, with the number of particles of different species [67,68]) rather than with energy or impact parameter. The radius R_o, which nontrivially combines space and time, shows a less clear scaling [11], retaining some energy dependence. As seen in Fig. 11, the radii from $p+p$ collisions at $\sqrt{s}=200$ GeV fall naturally in line with this multiplicity scaling. On the scale relevant to this comparison, the specific treatment of nonfemtoscopic correlations is unimportant.

One of the most important systematics in heavy ion femtoscopy is the m_T dependence of HBT radii, which directly measures space-momentum correlations in the emitting source at freeze-out; in these large systems, the m_T dependence is often attributed to collective flow [6]. As we saw in Fig. 6, a significant dependence is seen also for $p+p$ collisions. Several authors, e.g., [18,32,33,38,69], have remarked on the qualitative "similarity" of the m_T dependence of HBT radii measured in high-energy particle collisions, but the first direct comparison is shown in Fig. 12. There, the ratios of the three-dimensional radii in Au + Au collisions to $p+p$ radii obtained with different treatments of the nonfemtoscopic correlations are plotted versus m_T. Well beyond qualitative similarity, the ratios are remarkably flat; i.e., the m_T dependence in $p+p$ collisions is quantitatively almost identical to that in Au + Au collisions at RHIC. We speculate on the possible meaning of this in Sec. V B.

TABLE VII. Results from a fit to the 1D correlation function from $p+p$ collisions at $\sqrt{s}=200$ GeV using Eq. (6) to parametrize the femtoscopic correlations and Eq. (16) for nonfemtoscopic ones (EMCIC fit). The nonfemtoscopic parameters M_{1-4} were not varied, but kept fixed to the values in Table IV.

k_T (GeV/c)	$R_{\rm inv}$ (fm)	λ	χ^2/ndf
[0.15, 0.25]	1.38 ± 0.03	0.347 ± 0.005	99/27
[0.25, 0.35]	1.32 ± 0.03	0.354 ± 0.006	97/27
[0.35, 0.45]	1.23 ± 0.04	0.349 ± 0.009	86/27
[0.45, 0.60]	1.14 ± 0.05	0.411 ± 0.013	80/27

TABLE VIII. Results from a fit to the 1D correlation function from $p+p$ collisions at $\sqrt{s}=200$ GeV using Eq. (10) to parametrize the femtoscopic correlations and Eq. (14) for nonfemtoscopic ones. For each k_T cut, the parameters b and c were obtained from a fit to PYTHIA-generated correlation functions and then held fixed when fitting the experimental data. See text for details.

k_T (GeV/c)	$R_{\rm inv}$ (fm)	λ	b fixed	c fixed	χ^2/ndf
[0.15, 0.25]	1.29 ± 0.02	0.355 ± 0.007	−0.07	0.13	246/27
[0.25, 0.35]	1.23 ± 0.02	0.350 ± 0.006	−0.06	0.11	165/27
[0.35, 0.45]	1.16 ± 0.02	0.352 ± 0.007	−0.02	0.06	202/27
[0.45, 0.60]	1.08 ± 0.03	0.382 ± 0.010	−0.09	0.06	141/27

B. Results in the context of high-energy particle measurements

Recently, a review of the femtoscopic results [20] from particle collisions such as $p+p$, $p+\bar{p}$ and $e^+ + e^-$ studied at different energies has been published. Here, we compare STAR results from $p+p$ collisions at $\sqrt{s}=200$ GeV with world systematics.

The multiplicity dependence of femtoscopic parameters from one- and two-dimensional correlation functions are shown in Figs. 13 and 14. For any given experiment, the radius parameter increases with event multiplicity. However, in contrast to the nearly "universal" multiplicity dependence seen in heavy ion collisions (cf. Fig. 11), only a qualitative trend is observed when the different measurements are compared.

There are several possible reasons for this lack of universality [20]. Clearly one possibility is that there is no universal multiplicity dependence of the femtoscopic scales; the underlying physics driving the space-time freeze-out geometry may be quite different, considering $\sqrt{s}$ varies from 44 to 1800 GeV in the plot. However, even if there were an underlying universality between these systems, it is not at all clear that it would appear in this figure, due to various difficulties in tabulating historical data [20]. First, as discussed

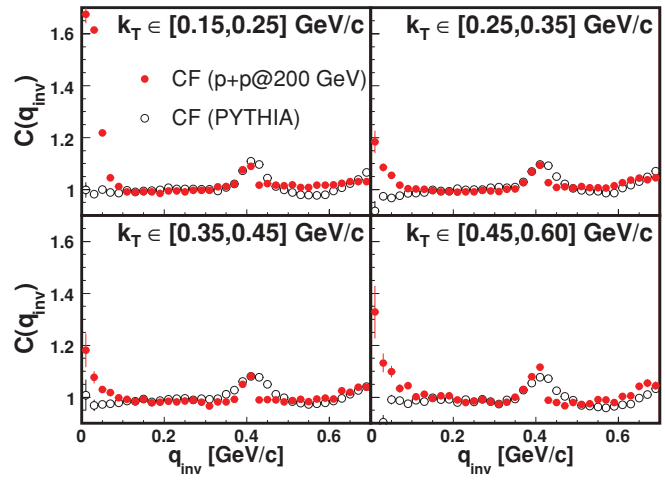

FIG. 7. (Color online) Correlation functions for oppositely signed pion pairs from minimum-bias $p+p$ collisions at $\sqrt{s_{NN}}=200$ GeV as measured by the STAR Collaboration (filled red circles) and as simulated with the PYTHIA event generator (open circles). See text for details.

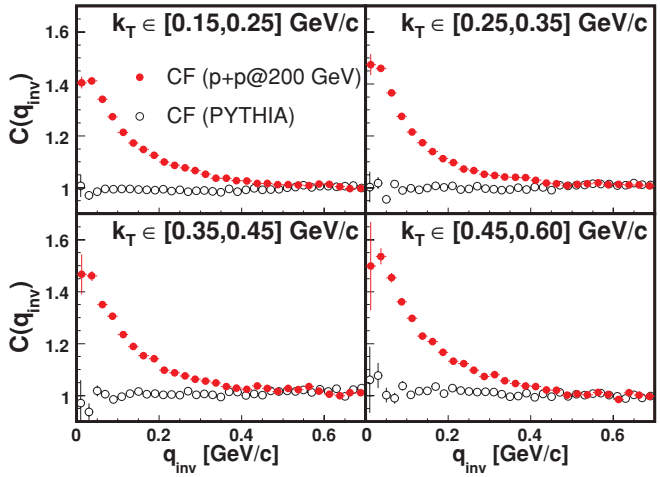

FIG. 8. (Color online) Same as Fig. 7, but for like-sign pions.

in Sec. II, the experiments used different fitting functions to extract the HBT radii, making direct comparison between them difficult. Second, as we have shown, the radii depend on both multiplicity and k_T. Since, for statistical reasons, the results in Fig. 11 are integrated over the acceptance of each experiment and these acceptances differ strongly, any universal scaling would be obscured. For example, since the acceptance of the Tevatron experiment E735 [38] is weighted toward higher k_T than the other measurements, one expects a systematically lower HBT radius at a given multiplicity. Indeed, even the universal multiplicity scaling in heavy ion collisions is only universal for a fixed selection in k_T. Third, the measure used to quantify the event multiplicity varies significantly in the historical literature; thus the determination of $\langle dN_{\rm ch}/d\eta\rangle$ for any given experiment shown in Fig. 11 is only approximate.

From the discussion above, we cannot conclude definitively that there is—or is not—a universal multiplicity scaling of femtoscopic radii in high-energy hadron-hadron collisions. We conclude only that an increase of these radii with multiplicity is observed in all measurements for which $\sqrt{s} \gtrsim 40$ GeV and that the present analysis of $p + p$ collisions is consistent with world systematics.

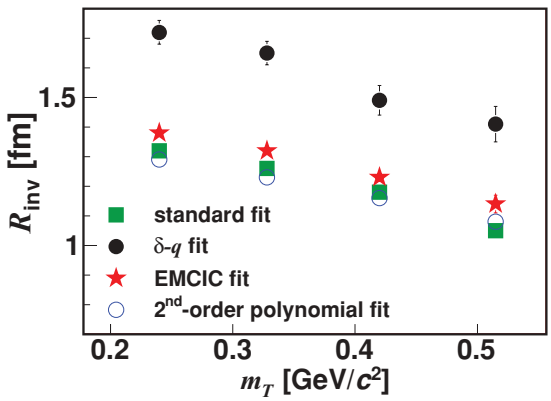

FIG. 9. (Color online) m_T dependence of $R_{\rm inv}$ from $p + p$ collisions at $\sqrt{s} = 200$ GeV for different parametrizations of the nonfemtoscopic correlations used in the fit procedure.

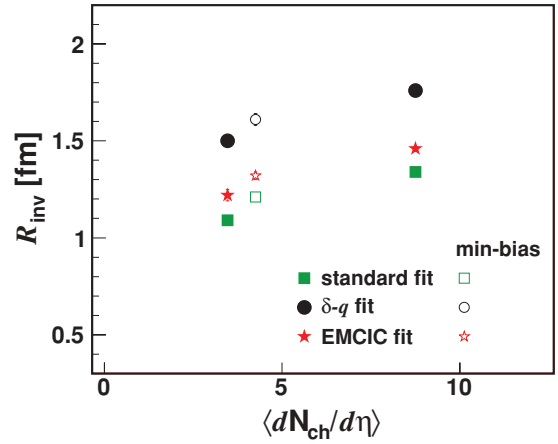

FIG. 10. (Color online) Multiplicity dependence of $R_{\rm inv}$ from $p + p$ collisions at $\sqrt{s} = 200$ GeV for different parametrizations of the nonfemtoscopic correlations. Pions within the range of $k_T = [0.15, 0.60]$ GeV/c were used in the analysis.

In Sec. IV, we discussed the p_T dependence of HBT radii observed in our analysis. Previous experiments on high-energy collisions between hadrons—and even leptons—have reported similar trends. As discussed above, direct comparisons with historical high-energy measurements are problematic. Comparisons between fit parameters to one- and two-dimensional correlation functions are shown in Figs. 15 and 16. All experiments observe a decrease in femtoscopic parameters with increasing transverse momentum. Our radii at $\sqrt{s} = 200$ GeV fall off similarly or somewhat more than those measured at an order of magnitude lower energy at the CERN Super Proton Synchrotron (SPS) [32,45], and less than those measured at an order of magnitude higher energy at the Tevatron [38]. It is tempting to infer that this compilation indicates an energy evolution of the p_T dependence of femtoscopic radii. However, given our previous discussion, we conclude only that there is qualitative agreement between experiments at vastly different collision energies, and all show similar p_T dependence.

Systematics in three-dimensional HBT radii from hadron collisions are less clear and less abundant, though our measurements are again qualitatively similar to those reported at the SPS, as shown in Fig. 17. There, we also plot recent results from $e^+ + e^-$ collisions at the CERN Large Electron–Positron Collider (LEP); in those 3D analyses, the longitudinal direction is the thrust axis, whereas the beam axis is used in hadron-hadron collisions, as in heavy ion collisions.

VI. DISCUSSION

We have seen that HBT radii from $p + p$ collisions at RHIC are qualitatively consistent with the trends observed in particle collisions over a variety of collision energies. Furthermore, they fall quantitatively into the much better defined world systematics for heavy ion collisions at RHIC and similar energies. Particularly intriguing is the nearly identical dependence on m_T of the HBT radii in $p + p$ and heavy ion collisions, as this dependence is supposed [26,75] to reflect the

TABLE IX. Multiplicity dependence of fit results to the 1D correlation function from $p+p$ collisions at $\sqrt{s} = 200$ GeV for different fit parametrizations.

Method	Fit parameter	$\langle dN_{\rm ch}/d\eta \rangle$		
		4.25 (min-bias)	3.47	8.75
standard fit	$R_{\rm inv}$ (fm)	1.21 ± 0.01	1.09 ± 0.02	1.34 ± 0.02
	λ	0.353 ± 0.003	0.347 ± 0.04	0.356 ± 0.03
	χ^2/ndf	202/27	100/27	92/27
δ-q fit	$R_{\rm inv}$ (fm)	1.61 ± 0.01	1.50 ± 0.03	1.76 ± 0.03
	λ	0.312 ± 0.003	0.275 ± 0.005	0.322 ± 0.007
	$\delta Q_{\rm inv}$ (c/GeV)	-0.191 ± 0.003	-0.242 ± 0.005	-0.194 ± 0.006
	χ^2/ndf	159/26	83/26	73/26
EMCIC fit	$R_{\rm inv}$ (fm)	1.32 ± 0.02	1.22 ± 0.03	1.46 ± 0.02
	λ	0.481 ± 0.003	0.485 ± 0.003	0.504 ± 0.004
	N	14.3 ± 4.7	11.8 ± 7.1	26.3 ± 8.4
	χ^2/ndf	161/26	80/26	75/26

underlying dynamics of the latter. Several possible sources of an m_T dependence of HBT radii in small systems have been put forward to explain previous measurements.

(i) Alexander *et al.* [76,77] have suggested that the Heisenberg uncertainty principle can produce the transverse momentum dependence of femtoscopic radii in $e^+ + e^-$ collisions. However, as discussed in Ref. [20], a more detailed study of the results from $e^+ + e^-$ collisions complicates the quantitative comparisons of the data from various experiments and thus the interpretation. Additionally, the arguments from Refs. [76,77] apply only to the longitudinal direction (R_l), so could not explain the dependence of all three radii.

(ii) In principle, string fragmentation should also generate space-momentum correlations in small systems, hence an m_T dependence of the HBT radii. However, there are almost no quantitative predictions that can be compared with data. The numerical implementation PYTHIA, which incorporates the Lund string model into the soft sector dynamics, implements Bose-Einstein enhancement only as a crude parametrization designed to mock up the effect (cf. Sec. 12.4.3 of Ref. [80]) for the purpose of estimating distortions to W-boson invariant mass spectrum. Any Bose-Einstein correlation function may be dialed into the model, with 13 parameters to set the HBT radius, λ parameter, and correlation shape; there is no first-principles predictive power. From a first-principles point of view, the strong mass dependence may pose a challenge to the Lund string model [81–83].

(iii) Long-lived resonances may also generate the space-momentum dependence of femtoscopic radii [84]. However, as discussed in Ref. [20], the resonances would affect the HBT radii from $p+p$ collisions differently than those from Au + Au collisions, since the scale of the resonance "halo" is fixed by resonance lifetimes while the scale of the "core" is different for the two cases. Thus it would have to be a coincidence that the same m_T dependence is observed in both systems. Nevertheless, this avenue should be explored further.

(iv) Białas *et al.* have introduced a model [85] based on a direct proportionality between the four-momentum and space-time freeze-out position; this model successfully described data from $e^+ + e^-$ collisions. The physical scenario is based on freezeout of particles emitted from a common tube, after a fixed time of 1.5 fm/c. With a very similar model, Humanic [86] was able to reproduce femtoscopic radii measured at the Tevatron [38] only with strong additional hadronic

TABLE X. Multiplicity dependence of fit parameters to two-dimensional correlation functions from $p+p$ collisions at $\sqrt{s} = 200$ GeV using Eqs. (7) and (8). To consistently compare with previous measurements, Ω was set to unity [cf. Eq. (5)].

Method	Fit parameter	$\langle dN_{\rm ch}/d\eta \rangle$		
		4.25 (min-bias)	3.47	8.75
Eq. (7)	R_B (fm)	1.79 ± 0.01	1.61 ± 0.02	1.92 ± 0.02
	τ (fm/c)	1.03 ± 0.02	0.98 ± 0.02	1.24 ± 0.03
	λ	0.353 ± 0.003	0.354 ± 0.003	0.334 ± 0.004
	χ^2/ndf	5308/896	2852/896	1890/896
Eq. (8)	R_G (fm)	1.01 ± 0.01	0.89 ± 0.01	1.07 ± 0.01
	τ (fm/c)	0.76 ± 0.01	0.73 ± 0.02	0.91 ± 0.02
	λ	0.353 ± 0.003	0.352 ± 0.003	0.332 ± 0.004
	χ^2/ndf	5749/896	3040/896	2476/896

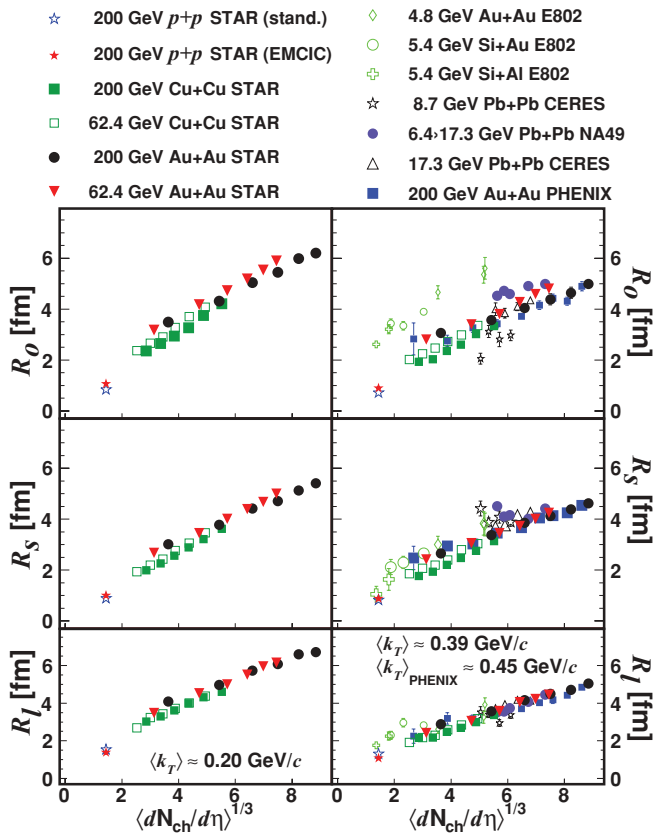

FIG. 11. (Color online) Multiplicity dependence of the HBT radii from $p + p$, Cu + Cu [56], and Au + Au [55,56] collisions from STAR compared with results from other experiments [11]. Left and right panels show radii measured with $\langle k_T \rangle \approx 0.2$ and 0.39 GeV/c, respectively. Radii from $p + p$ collisions are shown by blue (standard fit) and red (EMCIC fit) stars.

rescattering effects. With rescattering in the final state, both the multiplicity and the m_T dependence of the radii were reproduced [86].

(v) It has been suggested [18,32,33,38,87] that the p_T dependence of HBT radii in very small systems might reflect bulk collective flow, as it is believed to do in heavy ion collisions. This is the only explanation that would automatically account for the nearly identical p_T scaling discussed in Sec. V A. However, it is widely believed that the system created in $p + p$ collisions is too small to generate bulk flow.

The remarkable similarity between the femtoscopic systematics in heavy ion and hadron collisions may well be coincidental. Given the importance of the m_T dependence of HBT radii in heavy ion collisions, and the unclear origin of this dependence in hadron collisions, further theoretical investigation is clearly called for. Additional comparative studies of other soft-sector observables (e.g., spectra) may shed further light onto this coincidence.

VII. SUMMARY

We have presented a systematic femtoscopic analysis of two-pion correlation functions from $p + p$ collisions at RHIC. In addition to femtoscopic effects, the data show correlations

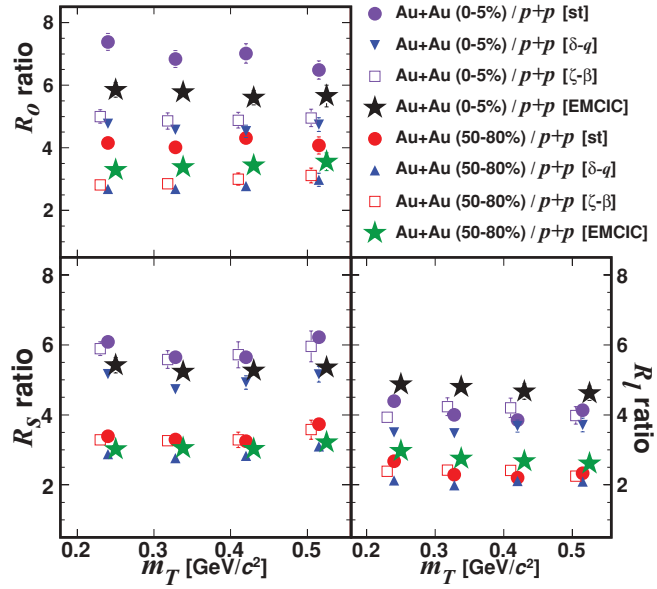

FIG. 12. (Color online) Ratio of the HBT radii from Au + Au collisions [55] to results from $p + p$ collisions plotted vs the transverse mass.

due to energy and momentum conservation. Such effects have been observed previously in low-multiplicity measurements at Tevatron, SPS, and elsewhere. A higher statistics analysis, which includes particle identification capability extended to higher momentum particles, is underway; with more than an order of magnitude greater statistics, the nonfemtoscopic correlations will be characterized with much more precision. To compare to historical data and to identify systematic effects on the HBT radii, we have treated these effects with a variety of empirical and physically motivated formulations. While the overall magnitude of the geometric scales vary with the method, the important systematics do not.

In particular, we observe a significant positive correlation between the one- and three-dimensional radii and the multiplicity of the collision, while the radii decrease with increasing transverse momentum. Qualitatively, similar multiplicity and momentum systematics have been observed previously in measurements of hadron and electron collisions at the SPS, Tevatron, Intersecting Storage Rings (ISR), and LEP colliders.

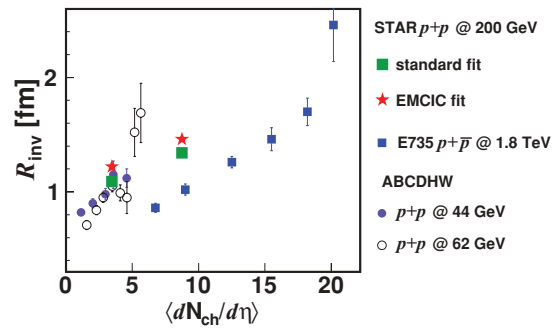

FIG. 13. (Color online) Multiplicity dependence of the 1D femtoscopic radius $R_{\rm inv}$ from hadronic collisions measured by STAR, E735 [38], and ABCDHW [70] collaborations.

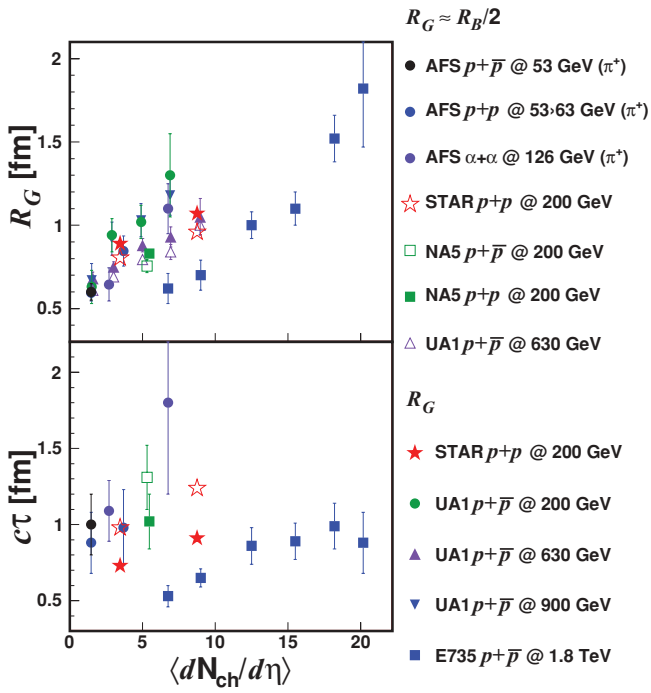

FIG. 14. (Color online) Multiplicity dependence of radius and time-scale parameters to two-dimensional correlation functions measured by STAR, E735 [38], UA1 [71], AFS [72], and NA5 [73]. The legend on the right indicates that the first seven sets of data points come from fits to Eq. (7), in which case the parameter $R_B/2$ is plotted in the upper panel; the last five sets of data points come from fits to Eq. (8), for which R_G is plotted. As discussed in Sec. II A and confirmed by STAR and UA1, $R_G \approx R_B/2$. The UA1 Collaboration set $\tau \equiv 0$ in their fits.

However, the results from these experiments could not be directly compared to those from heavy ion collisions, due to differences in techniques, fitting methods, and acceptance.

Thus, the results presented here provide a unique possibility for a direct comparison of femtoscopy in $p+p$ and $A+A$ collisions. We have seen very similar p_T and multiplicity scaling of the femtoscopic scales in $p+p$ as in $A+A$ collisions, independent of the fitting method employed. Given

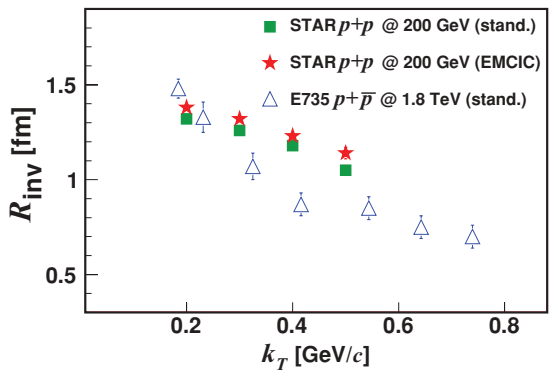

FIG. 15. (Color online) One-dimensional femtoscopic radii from $p+p$ collisions at RHIC and $p+\bar{p}$ collisions at the Tevatron [38] are plotted vs the transverse momentum $k_T \equiv (\vec{p}_{1,T} + \vec{p}_{2,T})/2$ [see Eq. (2)].

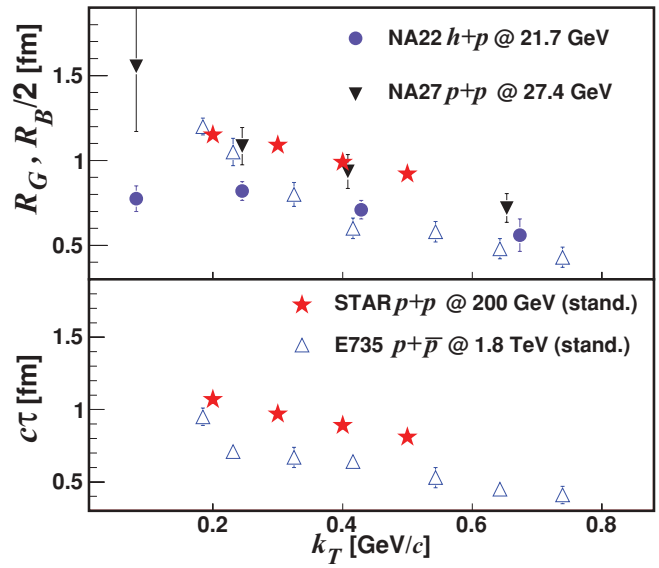

FIG. 16. (Color online) Transverse momentum dependence of fit parameters to two-dimensional correlation functions. STAR results from fit to Eq. (8), compared to measurements by E735 [38], NA27 [45], and NA22 [74]. The SPS experiments NA22 and NA27 set $\tau \equiv 0$ in their fits. STAR and E735 data are plotted vs $k_T \equiv (\vec{p}_{1,T} + \vec{p}_{2,T})/2$ [cf. Eq. (2)]. NA27 reported results in terms of $|\vec{P}|$ and NA22 in terms of $2|\vec{P}|$. For purposes of plotting here, $k_T \approx \sqrt{(2/3)}|\vec{P}|$ was assumed.

the importance of femtoscopic systematics in understanding the bulk sector in Au + Au collisions, further exploration of the physics behind the same scalings in $p+p$ collisions is clearly important to understand our "reference" system. The similarities observed could indicate a deep connection between

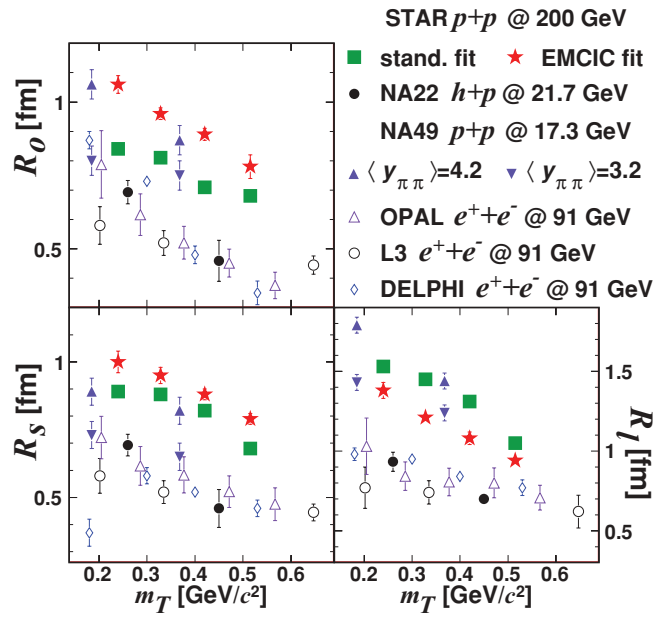

FIG. 17. (Color online) T ransverse mass dependence of 3D femtoscopic radii from particle collisions. Data from NA22 [32], NA49 preliminary [78], OPAL [33], L3 [44], and DELPHI [79].

the underlying physics of systems with size on the order of the confinement scale and of systems that are much larger. Similar comparative studies at RHIC and the Large Hadron Collider, where the higher collision energies will render conservation laws less important, will be most interesting in the quest to understand bulk dynamics of both hadronic and nuclear collisions.

ACKNOWLEDGMENTS

We thank the RHIC Operations Group and RCF at BNL, the NERSC Center at LBNL, and the Open Science Grid consortium for providing resources and support. This work was supported in part by the Offices of NP and HEP within the US DOE Office of Science, the US NSF, the Sloan Foundation, the DFG cluster of excellence 'Origin and Structure of the Universe' of Germany, CNRS/IN2P3, STFC and EPSRC of the United Kingdom, FAPESP CNPq of Brazil, Ministry of Ed. and Sci. of the Russian Federation, NNSFC, CAS, MoST, and MoE of China, GA and MSMT of the Czech Republic, FOM and NWO of the Netherlands, DAE, DST, and CSIR of India, Polish Ministry of Sci. and Higher Ed., Korea Research Foundation, Ministry of Sci., Ed. and Sports of the Republic of Croatia, and RosAtom of Russia.

[1] J. Adams *et al.* (STAR Collaboration), Nucl. Phys. A **757**, 102 (2005).
[2] K. Adcox *et al.* (PHENIX Collaboration), Nucl. Phys. A **757**, 184 (2005).
[3] B. B. Back *et al.* (PHOBOS Collaboration), Nucl. Phys. A **757**, 28 (2005).
[4] I. Arsene *et al.* (BRAHMS Collaboration), Nucl. Phys. A **757**, 1 (2005).
[5] E. Schnedermann, J. Sollfrank, and U. W. Heinz, Phys. Rev. C **48**, 2462 (1993).
[6] F. Retiere and M. A. Lisa, Phys. Rev. C **70**, 044907 (2004).
[7] J.-Y. Ollitrault, Phys. Rev. D **46**, 229 (1992).
[8] S. A. Voloshin, A. M. Poskanzer, and R. Snellings, arXiv:0809.2949.
[9] P. F. Kolb and U. Heinz, in *Quark Gluon Plasma 3*, edited by R. C. Hwa *et al.* (World Scientific, Singapore, 2003), p. 634, arXiv:nucl-th/0305084.
[10] R. Lednicky, Nucl. Phys. A **774**, 189 (2006).
[11] M. A. Lisa, S. Pratt, R. Soltz, and U. Wiedemann, Annu. Rev. Nucl. Part. Sci. **55**, 357 (2005).
[12] S. V. Akkelin and Y. M. Sinyukov, Phys. Lett. B **356**, 525 (1995).
[13] R. Lednicky, V. L. Lyuboshits, B. Erazmus, and D. Nouais, Phys. Lett. B **373**, 30 (1996).
[14] U. W. Heinz and P. F. Kolb, in *Proceedings of the 18th Winter Workshop on Nuclear Dynamics*, edited by R. Bellwied, J. Harris, and W. Bauer (EP Systema, Debrecen, Hungary, 2002), arXiv:hep-ph/0204061.
[15] S. Pratt, Phys. Rev. D **33**, 1314 (1986).
[16] D. H. Rischke and M. Gyulassy, Nucl. Phys. A **608**, 479 (1996).
[17] S. Bekele *et al.*, arXiv:0706.0537.
[18] W. Kittel, Acta Phys. Pol. B **32**, 3927 (2001).
[19] G. Alexander, Rep. Prog. Phys. **66**, 481 (2003).
[20] Z. Chajecki, Acta Phys. Pol. B **40**, 1119 (2009).
[21] G. I. Kopylov, Phys. Lett. B **50**, 472 (1974).
[22] P. Jacobs and X.-N. Wang, Prog. Part. Nucl. Phys. **54**, 443 (2005).
[23] F. Geurts *et al.* (STAR Collaboration), Nucl. Instrum. Meth. A **533**, 60 (2004).
[24] W. J. Llope *et al.* (STAR Collaboration), Nucl. Instrum. Meth. B **241**, 306 (2005).
[25] M. I. Podgoretsky, Sov. J. Nucl. Phys. **37**, 272 (1983).
[26] S. Pratt, Phys. Rev. Lett. **53**, 1219 (1984).
[27] G. Bertsch, M. Gong, and M. Tohyama, Phys. Rev. C **37**, 1896 (1988).
[28] P. Danielewicz and S. Pratt, Phys. Lett. B **618**, 60 (2005).
[29] P. Danielewicz and S. Pratt, Phys. Rev. C **75**, 034907 (2007).
[30] Z. Chajecki and M. Lisa, Phys. Rev. C **78**, 064903 (2008).
[31] P. Avery *et al.* (CLEO Collaboration), Phys. Rev. D **32**, 2294 (1985).
[32] N. M. Agababyan *et al.* (EHS/NA22 Collaboration), Z. Phys. C **71**, 405 (1996).
[33] G. Abbiendi *et al.* (OPAL Collaboration), Eur. Phys. J. C **52**, 787 (2007).
[34] J. L. Bailly *et al.* (NA23 Collaboration), Z. Phys. C **43**, 341 (1989).
[35] J. Uribe *et al.* (BNL-E766 Collaboration), Phys. Rev. D **49**, 4373 (1994).
[36] R. Lednicky and M. I. Podgoretsky, Sov. J. Nucl. Phys. **30**, 432 (1979).
[37] G. I. Kopylov and M. I. Podgoretsky, Sov. J. Nucl. Phys. **15**, 219 (1972).
[38] T. Alexopoulos *et al.* (E-735 Collaboration), Phys. Rev. D **48**, 1931 (1993).
[39] D. H. Boal, C. K. Gelbke, and B. K. Jennings, Rev. Mod. Phys. **62**, 553 (1990).
[40] S. Pratt, T. Csorgo, and J. Zimanyi, Phys. Rev. C **42**, 2646 (1990).
[41] M. G. Bowler, Phys. Lett. B **270**, 69 (1991).
[42] Y. Sinyukov, R. Lednicky, S. V. Akkelin, J. Pluta, and B. Erazmus, Phys. Lett. B **432**, 248 (1998).
[43] D. Buskulic *et al.* (ALEPH Collaboration), Z. Phys. C **64**, 361 (1994).
[44] P. Achard *et al.* (L3 Collaboration), Phys. Lett. B **524**, 55 (2002).
[45] M. Aguilar-Benitez *et al.* (LEBC-EHS Collaboration), Z. Phys. C **54**, 21 (1992).
[46] P. Abreu *et al.* (DELPHI Collaboration), Z. Phys. C **63**, 17 (1994).
[47] P. Abreu *et al.* (DELPHI Collaboration), Phys. Lett. B **286**, 201 (1992).
[48] K. Aamodt *et al.* (ALICE Collaboration), Phys. Rev. D **82**, 052001 (2010).
[49] Z. Chajecki, AIP Conf. Proc. **828**, 566 (2006).
[50] Z. Chajecki and M. Lisa, Phys. Rev. C **79**, 034908 (2009).
[51] D. A. Brown, A. Enokizono, M. Heffner, R. Soltz, P. Danielewicz, and S. Pratt, Phys. Rev. C **72**, 054902 (2005).
[52] W. Kittel and E. A. De Wolf, *Soft Multihadron Dynamics* (World Scientific, Singapore, 2005), see especially Sec. 11.5.
[53] C. Adler *et al.* (STAR Collaboration), Phys. Rev. Lett. **87**, 082301 (2001).

[54] J. Adams *et al.* (STAR Collaboration), Phys. Rev. Lett. **93**, 012301 (2004).
[55] J. Adams *et al.* (STAR Collaboration), Phys. Rev. C **71**, 044906 (2005).
[56] B. I. Abelev *et al.* (STAR Collaboration), Phys. Rev. C **80**, 024905 (2009).
[57] M. Anderson *et al.*, Nucl. Instrum. Meth. A **499**, 659 (2003).
[58] H. Bichsel, Nucl. Instrum. Meth. A **562**, 154 (2006).
[59] W. M. Yao *et al.* (Particle Data Group), J. Phys. G **33**, 1 (2006).
[60] A. Kisiel and D. A. Brown, Phys. Rev. C **80**, 064911 (2009).
[61] Torbjorn Sjostrand *et al.* Comput. Phys. Commun. **135**, 238 (2001).
[62] D. Miskowiec, (private communication).
[63] T. Sjostrand *et al.* PYTHIA 6.3 physics and manual, arXiv:hep-ph/0308153.
[64] R. D. Fields (CDF Collaboration), arXiv:hep-ph/0201192; CDF Note 6403 (unpublished); talks available from webpage [http://www.phys.ufl.edu/∼rfield/cdf/].
[65] H. Caines (STAR Collaboration), arXiv:1012.5008.
[66] H. Caines, Eur. Phys. J. C **49**, 297 (2007).
[67] D. Adamova *et al.* (CERES Collaboration), Phys. Rev. Lett. **90**, 022301 (2003).
[68] M. A. Lisa and S. Pratt, arXiv:0811.1352.
[69] T. Alexopoulos *et al.* (E-735 Collaboration), Phys. Lett. B **528**, 43 (2002).
[70] A. Breakstone *et al.* (Ames-Bologna-CERN-Dortmund-Heidelberg-Warsaw Collaboration), Z. Phys. C **33**, 333 (1987).
[71] C. Albajar *et al.* (UA1 Collaboration), Phys. Lett. B **226**, 410 (1989).
[72] T. Akesson *et al.* (Axial Field Spectrometer Collaboration), Phys. Lett. B **129**, 269 (1983).
[73] C. De Marzo *et al.*, Phys. Rev. D **29**, 363 (1984).
[74] N. M. Agababyan *et al.* (EHS-NA22 Collaboration), Z. Phys. C **59**, 195 (1993).
[75] U. W. Heinz and B. V. Jacak, Annu. Rev. Nucl. Part. Sci. **49**, 529 (1999).
[76] G. Alexander, I. Cohen, and E. Levin, Phys. Lett. B **452**, 159 (1999).
[77] G. Alexander, Phys. Lett. B **506**, 45 (2001).
[78] R. Ganz (NA49 Collaboration), Nucl. Phys. A **661**, 448 (1999).
[79] A. Smirnova (1999), in *Soft Multihadron Dynamics*, edited by N. G. Antoniou *et al.* (World Scientific, Singapore, 1999), p. 157.
[80] T. Sjostrand, S. Mrenna, and P. Skands, J. High Energy Phys. 05 (2006) 026.
[81] B. Andersson, in Proceedings of the 35th Rencontres de Moriond, 2000 (unpublished).
[82] G. Alexander, arXiv:hep-ph/0108194.
[83] G. Alexander, Acta Phys. Pol. B **35**, 69 (2004).
[84] U. A. Wiedemann and U. W. Heinz, Phys. Rev. C **56**, 3265 (1997).
[85] A. Bialas, M. Kucharczyk, H. Palka, and K. Zalewski, Phys. Rev. D **62**, 114007 (2000).
[86] T. J. Humanic, Phys. Rev. C **76**, 025205 (2007).
[87] T. Csorgo, M. Csanad, B. Lorstad, and A. Ster, Acta Phys. Hung. A **24**, 139 (2005).